Formation of the Ce-Nd mantle array: crustal extraction vs. recycling by subduction

Claudine Israel, M. Boyet, R. Doucelance, P. Bonnand, P. Frossard, D. Auclair, A. Bouvier

Formation of the Ce-Nd mantle array: crustal extraction vs. recycling by subduction

C. Israel[a,*], M. Boyet[a], R. Doucelance[a], P. Bonnand[a], P. Frossard[a], D. Auclair[a], A. Bouvier[b,c]

[a] Université Clermont Auvergne, CNRS, IRD, OPGC, Laboratoire Magmas et Volcans, F-63000 Clermont-Ferrand, France.

[b] Department of Earth Sciences, University of Western Ontario, Canada.

[c] Bayerisches Geoinstitut, Universität Bayreuth, Germany.

*Corresponding author.

E-mail address: claudine.israel@uca.fr (Claudine Israel).

ABSTRACT

We present new measurements of $^{138}Ce/^{142}Ce$ and $^{143}Nd/^{144}Nd$ isotopic ratios in terrestrial and extra-terrestrial samples. The mean value obtained from nine chondrites defines the $^{138}Ce/^{142}Ce$ ratio of the chondritic uniform reservoir (CHUR) as 0.02256577 ± 66 (2sd). MORBs and OIBs define the mantle array in the εNd vs. εCe diagram to be $\varepsilon Nd = -7.3\ (\pm 0.5) \times \varepsilon Ce + 0.4\ (\pm 0.3)$. From MORB measurements, we derive the isotopic composition of the depleted MORB mantle (DMM) to be $\varepsilon Ce = -1.1 \pm 0.6$ (2sd). Both CHUR and a modelled early-depleted mantle reservoir plot on the mantle array. Thus, the precise determination of the mantle array does not further constrain the La/Ce and Sm/Nd ratios of the bulk silicate Earth (BSE; i.e., primitive mantle). The composition of 1.8 Ga upper continental crust obtained from aeolian sediments is $\varepsilon Ce = 1.8 \pm 0.3$ (2sd; $\varepsilon Nd = -11.2$), and that of its 2.2 Ga equivalent is $\varepsilon Ce = 2.3 \pm 0.3$ (2sd; $\varepsilon Nd = -17$). Binary mixing models between depleted (DMM) and enriched (upper crust or mafic crust composition) components do not reproduce the linear Ce-Nd mantle array but plots close to the island arc basalt data. When the bulk Ce isotopic composition of the

continental crust is calculated from the range of accepted Nd isotope values and a mass-balance budget of the BSE, the mixing curves are closer to the mantle array. However the calculated Ce isotopic composition for the bulk crust is always less radiogenic than measurements. Adjusting the Ce-Nd isotopic composition or the Ce/Nd ratio of the end-members to fully linearise the mixing curve leads to unrealistic values never measured in terrestrial samples. We propose a recycling model to reconstruct the mantle array with the participation of both oceanic crust and sediments in the mantle through time. Cerium is a redox sensitive element, making the La-Ce and Sm-Nd systematics an ideal combination to investigate sediment recycling through time. In this recycling model, the most extreme EM-like signatures require the involvement of oceanic sediments that formed under reduced conditions before the Great Oxygenation Event at 2.4 Ga, and which are devoid of Ce elemental anomalies.

1. Introduction

Long-lived isotope systematics are remarkable tracers of the long-term evolution of the different terrestrial reservoirs. Radiometric systems based on refractory lithophile elements are the most likely to provide robust information on the bulk silicate Earth (BSE) because they were not lost during Earth's accretion or segregated into the core during its differentiation. Indeed, rare earth elements (REEs) have high condensation temperatures and remain strictly lithophile at the conditions of Earth's core formation (Bouhifd et al., 2015). The REE concentrations of the primitive mantle (PM) are assumed to be equivalent to those of the BSE, and their ratios should be chondritic if chondrites are the Earth's main building blocks. Boyet and Carlson (2005) identified a systematic offset between the $^{142}Nd/^{144}Nd$ ratios of modern terrestrial rocks and chondrites resulting in an active debate on the refractory lithophile element composition of the PM (see Caro et al., 2008; Jackson and Jellinek, 2013; O'Neill and Palme,

55 2008). ^{142}Nd is a radiogenic isotope partly produced by the decay of ^{146}Sm (T$_{1/2}$=103 Ma). Variations in

56 the ^{142}Nd abundances exist among Solar System materials and they reflect isotopic heterogeneities

57 within the protoplanetary disk (Bouvier and Boyet, 2016; Burkhardt et al., 2016). Determining terrestrial

58 variations relative to chondrites thus requires precise knowledge of the nature of Earth's building blocks.

59 Isotopic similarities between terrestrial samples and enstatite chondrites (ECs) suggest this group of

60 chondrites to be the main terrestrial component (Dauphas, 2017; Javoy, 1995). The mean EC ^{142}Nd/^{144}Nd

61 value is nevertheless lower than that of the BSE without distinguishable variations in their non-

62 radiogenic Nd isotopic compositions from Earth (Burkhardt et al., 2016; Boyet et al., 2018). Variations

63 in ^{142}Nd/^{144}Nd values between different EC subgroups show further that the EL3 subgroup matches the

64 terrestrial value (Boyet et al., 2018). These results remove the need of an early fractionation of the

65 Sm/Nd ratio of the Earth if the Earth was purely made of EL3 materials. The EL3 chondrites are

66 nevertheless problematic in regards to the elemental composition (e.g. Mg/Si) of the bulk Earth.

67 This study presents measurements of two long-lived isotopic systems in which both the parent and

68 daughter elements are REEs. ^{138}La decays into ^{138}Ce by beta emission ($t_{1/2,\beta}$ = 295.5 Gyr: Tanimizu,

69 2000) and into ^{138}Ba by electron capture, whereas ^{147}Sm decays into ^{143}Nd by alpha emission ($t_{1/2,\alpha}$ = 106

70 Gyr: Begemann et al., 2001). Variations of ^{138}Ce/^{142}Ce ratios are expected to be small due to the long

71 half-life and low abundance (0.09% of total La) of ^{138}La. The latest generation of thermal ionisation

72 mass spectrometers (TIMS) can achieve long-term analytical errors below 30 ppm on ^{138}Ce/^{142}Ce

73 (Bonnand et al., 2019), allowing characterisation of Ce isotopic variations in terrestrial and

74 extraterrestrial materials. Here we present analyses of 11 chondrites (ordinary, enstatite, and

75 carbonaceous) that we use to estimate the Ce isotopic composition of the chondritic uniform reservoir

76 (CHUR). We also redefine the Ce-Nd mantle array based on previous and new measurements including

77 seven mid-ocean ridge basalts (MORBs) and 51 ocean island basalts (OIBs). Lastly, we report the first

78 Ce-Nd isotopic compositions of loess samples as a proxy for the upper continental crust (UCC).

79

80 Dickin (1987) first used the Ce-Nd isotopic correlation defined by OIBs to estimate the Ce isotopic

81 composition of the BSE. His regression intercepts the CHUR Nd isotopic composition at a BSE Ce

82 isotopic composition that is 60 ppm less radiogenic than the CHUR value defined by Shimizu et al.

83   (1984). However, new results from chondrites and mantle-derived samples lead to a different

84   observation. The mantle array passes directly through the CHUR composition in the Ce-Nd isotopic

85   diagram (Willig and Stracke, 2019). Our new results first confirm this trend. Moreover we show that a

86   modelled reservoir depleted in incompatible elements (and characterised by a depleted REE pattern; see

87   early-depleted reservoir in Boyet and Carlson, 2005) that would be formed early in the Solar System's

88   history also plots on the mantle array.

89

90   The mantle array must reflect the formation of the major silicate reservoirs and their interactions during

91   Earth's history. Important questions have been addressed by coupling Lu-Hf and Sm-Nd isotope

92   systematics; for example, arc lavas do not follow the Hf-Nd mantle array, which reflects the elevated

93   ^{176}Hf/^{177}Hf signature measured in most oceanic sediments (Carpentier et al., 2009). Also, the presence

94   of pelagic sediments in the source of the Hawaiian hotspot was first identified from Hf-Nd isotopic

95   measurements (Blichert-Toft et al., 1999). Cerium is a redox sensitive element, making the La-Ce and

96   Sm-Nd systematics an ideal combination to investigate sediment recycling through time. Indeed, most

97   documented modern forearc sediments are depleted in Ce relative to neighbouring elements (Plank,

98   2014). Before the Great Oxygenation Event (GOE), however, all REEs should have behaved similarly

99   and no Ce fractionation is expected to have occurred during that time. Coupling Ce and Nd isotopic

100   measurements will thus provide additional constraints on the nature of sediments recycled into the deep

101   mantle and sampled via hotspot volcanism. Chauvel et al. (2008) explained the Hf-Nd mantle array by

102   the recycling of oceanic crust and sediments into the mantle. Here, we present similar models in Ce-Nd

103   isotope diagrams for the first time.

104

105

106   **2. Sample selection**

107

108   We measured the Ce and Nd isotopic compositions of four ordinary chondrites, six enstatite chondrites,

109   one carbonaceous chondrite, seven MORBs, 51 OIBs, one intraplate continental volcanism occurrence

110   (Ethiopia), and six loess samples. To include all mantle end-members, we selected rocks with extreme

4

Nd-Sr-Pb-He compositions. OIB samples were selected from 13 locations covering the Atlantic (Iceland, São Miguel (Azores archipelago), Cape Verde, Saint Helena, Tristan Da Cunha), Pacific (Hawaii, MacDonald seamount, Rurutu and Tubuai Islands (Austral archipelago), Fangataufa (Tuamotu archipelago), Tahaa Island (Society archipelago)), and Indian Oceans (Heard, Kerguelen, Reunion and Saint-Paul Island (French Southern and Antarctic Lands)). MORB samples are unaltered glasses collected on the Pacific ridge (Bellot et al., 2015) and the Southwest Indian Ridge. The Pacific MORBs have similar REE patterns and do not show the Dupal anomaly (Sr and Pb isotopic anomalies in MORBs and OIBs erupted around 30° S). We used loesses from western Europe (wind-transported periglacial deposits), China and Tajikistan (sediments originating in northwestern Mongolia and the Karakum (Turkmenistan) and Kyzylkum deserts (Kazakhstan and Uzbekistan), respectively), and the Sahara Desert (dusts blown to Southern France; Chauvel et al., 2014 and references therein; Supplementary data 1, Figs S1-4).

3. Analytical procedures

3.1. Dissolution and chromatography protocols

All samples were entirely processed at the Laboratoire Magmas et Volcans (LMV, Clermont-Ferrand, France), except three chondrites (NWA 8007, NWA 10854, and Adrar Bous) that were dissolved at the University of Western Ontario (UWO). Mantle-derived and loess samples were dissolved using the following protocol. We used 50 to 300 mg of sample depending on the REE concentration and the quantity of powder available. Powders were digested in a 3:1 mixture of HF (65%) and HNO_3 (48%) that was maintained at 75 °C on a hot plate for 48 h. Once dried, the samples were dissolved a second time in 6 M HCl. The dissolution protocol was slightly different for chondrites. Oudiyat Sbaa, Yilmia, Pillistfer, Agen, Sahara 97158, and Saint-Séverin were dissolved in a 10:1 mixture of HF (65%) and HNO_3 (48%) in PFA-Savillex beakers placed on a hot plate at 110 °C for seven days. Fluorides were broken down in a second step using concentrated $HClO_4$. Allende, Sahara 97072, Adrar Bous, NWA

138   8007, and NWA 10854 were dissolved in Parr bombs using the same acid mixtures (48 hours at 180 °C

139   in HF-HNO$_3$, or seven days at 150 °C, followed by HClO$_4$ treatment). Once dried, all chondrite samples

140   were dissolved in 6 M HCl for two to five days on a hot plate at 110 °C.

141

142   All sample solutions were then separated into two aliquots for trace element and isotopic dilution (5–

143   10%) and Ce-Nd isotopic analyses (90–95%). Ce and Nd were chemically separated following the

144   procedure reported in detail by Bonnand et al., 2019; modified from Tazoe et al., 2007 and Bellot et al.,

145   2015 and summarised here. REEs (including Ba) were first separated from the matrix using AG50W-

146   X8 resin. An additional step using AG1-X8 resin (200–400 mesh) was performed on the meteorites to

147   remove Fe. Then, Ce was separated from the trivalent REEs using an oxidation technique (NaBrO$_3$) on

148   Ln-Spec resin, and purified in a final step using AG50W-X8 resin to remove any residual Ba. The

149   remaining REE fraction was processed using Ln-Spec resin (25–50 mesh) and Nd was collected in 0.25

150   M HCl. Total procedural blanks for Ce and Nd were 0.4 ± 1.7 ng (2sd, n = 12) and 0.02 ± 0.05 ng (2sd,

151   n = 7), respectively, and were always negligible relative to the quantities collected from the samples.

152

153   3.2.   Trace element concentrations and Ce and Nd isotopic measurements

154

155   We determined trace element abundances for all samples except NWA 8007, NWA 10854, and Adrar

156   Bous by inductively coupled plasma mass spectrometry (ICP-MS) using the Agilent 7500 quadrupole

157   instrument in normal mode (no collision cell) at LMV. These 3 meteorites were analysed using a Thermo

158   iCAP quadrupole ICP-MS in collision cell mode with He flux at UWO. Concentrations were calculated

159   using an external calibration (CMS reference material standard, Inorganic Ventures). We analysed

160   certified rock standard BHVO-2 (or BCR-2 at UWO) together with our samples to assess the accuracy

161   of our analytical protocol.

162

163   We performed Ce isotopic analyses in static mode with double Re filaments on a ThermoScientific^{TM}

164   Triton Plus TIMS at LMV. Ce isotopes were measured as CeO$^+$ oxides using the procedure described

165   in Bonnand et al. (2019). A typical run comprised 27 blocks with 20 cycles of 8 s integration time each,

166   and a baseline measurement (deflected ion beams) of 60 s. Matrix rotation of the amplifiers was not

167   active because the 10^{11}, 10^{12}, and 10^{13} Ω resistors were used simultaneously. All corrections (oxygen,

168   mass discrimination using $^{136}Ce/^{142}Ce = 0.01688$, and tailing effect) were performed offline. All reported

169   uncertainties are 2 standard deviations. During the course of the study, the value of the tailing correction

170   was $\Delta\varepsilon Ce = 0.77 \pm 0.18$ ($n = 151$). Repeated measurements of our Ce_{LMV} synthetic reference material

171   gave $^{138}Ce/^{142}Ce = 0.02257063 \pm 54$ (24 ppm; $n = 31$). $^{138}Ce/^{142}Ce$ ratios measured for rock reference

172   standards BCR-2 and BHVO-2 were equal to 0.02256684 ± 48 (21 ppm; $n = 9$) and 0.02256453 ± 99

173   (44 ppm; $n = 7$), respectively (see Supplementary data 2 for details on the total reproducibility of

174   measurements). The mean $^{134}Ba^{16}O$ signal was 0.000003 ± 0.000010 V ($n = 139$), and the maximum

175   reached 1×10^{-5} V, which has no significant effect on the $^{138}Ce/^{142}Ce$ and $^{136}Ce/^{142}Ce$ ratios. Ce isotopic

176   compositions of loess samples were measured on the same TIMS but using the two-line acquisition

177   method of 360 cycles (Bellot et al., 2015).

178

179   We performed Nd isotopic analyses in static mode with double Re filaments using a ThermoScientific^{TM}

180   Triton TIMS at LMV. A typical run comprised 18 blocks of 10 cycles, allowing a full rotation of the

181   amplifier system. Mass discrimination was corrected using $^{146}Nd/^{144}Nd = 0.7219$. Repeated

182   measurements of the JNdi-1 standard and the two rock reference standards BCR-2 and BHVO-2 gave

183    $^{143}Nd/^{144}Nd = 0.512099 \pm 4$ (7 ppm; $n = 16$), 0.512623 ± 8 (17 ppm; $n = 3$) and 0.512973 ± 3 (6 ppm; n

184    $= 3$), respectively. The Sm contribution measured at mass 147 was negligible in all analyses.

185

186

187   **4. Results**

188

189   Measured Ce and Nd isotopic compositions are reported in Table 1 and 2, and details for individual runs

190   (number of cycles, mean intensity, tailing value) are given in Supplementary data 2.

191

4.1. Chondrites

Chondrites define a small range of $^{138}Ce/^{142}Ce$ ratios between 0.02256522 and 0.02256633, excluding the two EL6 samples (Yilmia and Pillistfer) that show lower values (0.02256251 and 0.02256272, respectively). Enstatite, ordinary, and carbonaceous chondrites have indistinguishable average values within errors (Fig. 1A). The two EL6 samples plot on the 4.568 Ga isochron in the $^{138}Ce/^{142}Ce$ vs. La/Ce diagram (Fig. 1B) suggesting that their La/Ce ratios were modified early in the history of the Solar System, in agreement with previous conclusions (Barrat et al., 2014; Boyet et al., 2018). Consequently, we define the Ce isotopic composition of CHUR as the mean value of the other nine (i.e., unmodified) chondrite samples: $^{138}Ce/^{142}Ce_{CHUR}$ = 0.02256577 ± 66 (29 ppm).

To compare our CHUR value with the most recent estimates of Bellot et al. (2015) and Willig and Stracke (2019), we have normalised these previous data using a common reference material ($^{138}Ce/^{142}Ce_{CeLMV}/^{138}Ce/^{142}Ce_{CeAMES}$ = 0.02257053/0.02257426, Bonnand et al., 2019). The normalised CHUR value of Willig and Stracke (2019) is thus $^{138}Ce/^{142}Ce$ = 0.02256644 ± 53 (using $^{136}Ce/^{142}Ce$ = 0.01688), consistent with our estimate within errors. In contrast, the normalised CHUR value of Bellot et al. (2015) is significantly distinct from our value (Fig 1A). Combining the normalised data of Willig and Stracke (2019) with our measurements to calculate a mean chondritic $^{138}Ce/^{142}Ce$ ratio increases the uncertainty from 29 to 39 ppm because their chondrite measurements were systematically 30 ppm more radiogenic than ours. This deviation exists also for MORB and OIB data and it is highlighted when data are reported in a $^{143}Nd/^{144}Nd$ vs. $^{138}Ce/^{142}Ce$ isotope diagram. Thus, to compare these different datasets, we henceforth strictly use the epsilon notation (Fig. 1B). In the future, to achieve better interlaboratory reliability, chondrites should be measured under similar analytical conditions (see Supplementary Fig. S5).

4.2. Ce-Nd isotopic compositions of terrestrial samples

219   The Ce and Nd isotopic compositions of terrestrial samples measured in this study are reported in a εNd

220   vs. εCe diagram (Fig. 2) and compared with recent MORB and OIB data from the literature. MORB

221   samples have the least radiogenic Ce ratios and the most radiogenic Nd ratios, with εCe and εNd values

222   ranging from –1.19 to –0.71 and from 8.85 to 10.42, respectively. Pacific MORBs have slightly lower

223   Ce isotopic ratios than Indian ones. OIB samples define larger compositional ranges with εCe and εNd

224   values ranging from –1.44 to 0.43 and from –2.49 to 10.42, respectively. Enriched mantle (EM1 and

225   EM2)-like OIBs (Heard, Gough, Kerguelen, Tristan Da Cunha, São Miguel, and Tahaa) have the highest

226   Ce isotopic ratios. Samples from Iceland and two samples from Hawaii plot in the MORB field. Other

227   OIBs, including those with HIMU affinity (Saint-Helena), have compositions intermediate between

228   Iceland samples and those with EM affinities, forming a continuum between these two end-members.

229   The seven samples from Ethiopia have subchondritic εCe values and plot along the OIB trend. The

230   entire range of MORB εCe values is relatively large (1 unit) compared to OIBs (1.5 units) considering

231   the dispersion of εNd values (3 units for MORBs and 12 units for OIBs).

232

233   Loess samples have εCe and εNd values ranging from 1.6 to 2.0 and from –13.52 to –9.73, respectively,

234   with average values of εCe = 1.8 ± 0.3 and εNd = –11.2 ± 3.0. Our samples represent a sub-sampling of

235   those analysed by Chauvel et al. (2014), who determined a mean εNd value of –10.3 ± 2.3, consistent

236   with our results.

237

238   **5. Discussion**

239   5.1.   Definition of the Ce-Nd mantle array

240

241   Dickin (1987) was the first to present coupled Ce and Nd isotopic measurements of OIB samples and

242   define the Ce-Nd mantle array. Recently, Willig and Stracke (2019) published new high-precision

243   measurements of MORBs and OIBs and refined the εCe-εNd correlation. We extended their results by

244   analysing 66 new mantle-derived samples. The regression line calculated from all samples presented in

245   Figure 2 (n = 134) gives the following equation for the mantle array: εNd = -7.3 (± 0.5) × εCe + 0.4 (±

246   0.3), using Isoplot® and considering errors of 0.25 for εCe and 0.10 for εNd. In agreement with Willig

247   and Stracke (2019), the mantle array intercepts the chondritic composition. However, we will show in

248   the following section that a chondritic intercept for the mantle array does not prove that these mantle-

249   derived samples come from a source with a chondritic light REE (LREE) pattern.

250

251   5.2.   Chondritic vs. non-chondritic REE composition of the primitive mantle

252

253   A non-chondritic REE composition of the primitive mantle was initially proposed to explain the

254   radiogenic εNd values measured in Eoarchean samples (e.g., Chase and Patchett, 1988). High-precision

255   isotopic measurements of the short-lived ^{146}Sm-^{142}Nd systematics in both terrestrial samples and

256   chondrites have strongly revived the debate on the nature of the REE composition of the PM (Boyet and

257   Carlson, 2005). Most ^{142}Nd/^{144}Nd variations measured in the different chondrite groups are now

258   attributed to initial isotopic heterogeneities of nucleosynthetic origin within the solar nebula during

259   planetary accretion (Bouvier and Boyet, 2016; Burkhardt et al., 2016; Carlson et al., 2007). However,

260   in terms of non-radiogenic Nd isotope compositions, enstatite chondrites are the closest to the Earth and,

261   on average, are depleted in ^{142}Nd by 10 ppm relative to terrestrial samples (Boyet et al., 2018; Dauphas,

262   2017) with the exception of the EL3 sub-group. Carbonaceous chondrites may have been involved

263   during the last stage of Earth's accretion, and, because they are depleted in ^{142}Nd by 32 ppm relative to

264   terrestrial samples, they may have further contributed to the difference between terrestrial and EC values

265   (Boyet et al., 2018). None of the current meteorite groups available for analysis and mixing models

266   satisfy the isotopic and elemental composition of the Earth, and call for unknown end-members or

267   fractionation processes. Thus, it is still possible that some of the observed difference between terrestrial

268   and chondritic ^{142}Nd abundances was produced by the decay of ^{146}Sm in a superchondritic Sm/Nd

269   reservoir.

270

271   To attempt to constrain the REE composition of the PM, we consider a 10 ppm increase in radiogenic

272   ^{142}Nd that corresponds to the difference between modern terrestrial samples and either EC values having

273　a terrestrial mean ^{142}Nd/^{144}Nd 10 ppm higher than that of the continental crust, or an Earth made with

274　90% of EL3 chondrites + 10% carbonaceous chondrites (Boyet et al., 2018). This excess ^{142}Nd would

275　have been produced in a high-Sm/Nd reservoir. Assuming this reservoir formed 4.568 Ga, this

276　corresponds to a 3.6% increase of the BSE Sm/Nd ratio relative to the chondritic value. Modelled Sm/Nd

277　ratios in early-differentiated reservoirs have been discussed in a large number of publications (e.g. Boyet

278　and Carlson, 2005; Caro et al., 2008) and can goes up to 5% higher if this early-differentiated reservoir

279　formed 4.5 Ga. Here we use the terms "early depleted reservoir" (EDR) and "early enriched reservoir"

280　(EER) as defined by Boyet and Carlson (2005): the EDR has a chondrite-normalised REE pattern that

281　is depleted in LREEs relative to heavy REEs and thus a superchondritic Sm/Nd ratio, whereas the

282　complementary EER has a subchondritic Sm/Nd ratio. The EER may exist in the lower mantle (Boyet

283　and Carlson, 2005) or may correspond to embryonic crust lost by collisional erosion during Earth's

284　accretion (O'Neill and Palme, 2008).

285

286　We calculate the REE composition of the EDR by the method developed by Jackson and Jellinek (2013),

287　which is based on three different isotopic systematics (^{146}Sm-^{142}Nd, ^{147}Sm-^{143}Nd, and ^{176}Lu-^{176}Hf) and

288　invariant elemental ratios (e.g., Sm/Hf). CHUR REE elemental ratios needed for this calculation were

289　obtained from a large and recent database of ordinary, enstatite, and carbonaceous chondrites (Barrat et

290　al., 2012, 2014; Boyet et al., 2018; Braukmüller et al., 2018; Dauphas and Pourmand, 2015; Pourmand

291　et al., 2012). We selected the least thermally metamorphosed fall samples (types 1–4, n = 42), and

292　outliers (Orgueil and Kelly) were removed. The mean La/Ce ratio thus calculated for CHUR is 0.387 ±

293　0.022 (n = 39), similar to the value we obtained from our smaller sample set (La/Ce$_{CHUR}$ = 0.390 ±

294　0.022). The CHUR Sm/Nd ratio determined from the same database of chondrite samples is 0.324 ±

295　0.014, consistent with the value proposed by Bouvier et al. (2008). Lastly, we used the Lu/Hf ratio of

296　CHUR (0.236) calculated from the average ^{176}Lu/^{177}Hf value determined by Bouvier et al. (2008).

297

298　The calculated REE pattern for an EDR is presented in Figure 3. For a 3.6% increase of the Sm/Nd ratio

299　of the BSE, the modelled EDR has εCe = –0.4 and εNd = 4.1. This reservoir plots very close to the

300　mantle array in the εNd vs. εCe diagram, and shows Ce-Nd isotopic compositions similar to those

301 measured in several OIBs (Fig. 4). A large-scale silicate differentiation event early in the Solar System's

302 evolution does not produce any offset in the Ce-Nd isotopic composition of the EDR relative to the

303 mantle array. Thus, defining the Ce-Nd mantle array does not resolve the long-standing debate over the

304 chondritic vs. EDR-like REE composition of the PM.

305

306 5.3. Crustal extraction mass-balance calculations

307

308 Mantle melting and subsequent extraction of the crust has contributed to the depletion of the mantle in

309 incompatible elements. Crustal growth models are widely discussed and several authors have proposed

310 rapid continental growth early in Earth's history despite the scarce geological record of the Earth's first

311 billion years (Belousova et al., 2010; Dhuime et al., 2012). Geochemical signatures in mantle-derived

312 samples linked to this process are particularly difficult to decipher because surface material is

313 continuously reintegrated into the mantle via subduction. In this section, to investigate the production

314 of the various mantle reservoirs, we attempt to recreate the Ce-Nd mantle array via mass-balance mixing

315 calculations between the depleted MORB mantle (DMM) and continental crust (CC). We first simplify

316 our approach by assuming that the CC was extracted from the PM in a single differentiation step (i.e.,

317 DMM + CC = BSE). Since we have not resolved the chondritic vs. EDR-like composition of the PM,

318 we explore both bulk compositions and compare their modelled Ce-Nd mixing curves to the mantle

319 array. Distinct scenarios proposed that oceanic crust formation was the dominant process of mantle

320 depletion with continents formed later by reworking in subduction zones (e.g., Jones et al., 2019).

321 Furthermore, isotopic studies of rocks from the Nuvvuagittuq Supracrustal Belt and the neighbouring

322 Hudson Bay terrane show that the Archean felsic crust formed by reworking of Hadean mafic crust

323 (O'Neil et al., 2019; O'Neil and Carlson, 2017). From these observations, we choose to calculate the

324 Ce-Nd isotopic composition of such an enriched reservoir and compare it to the global dataset to evaluate

325 the effect of primitive mafic crustal extraction on the mantle.

326

327 5.3.1. End-members

328 ***Depleted MORB Mantle***

329   The DMM end-member isotopic composition is commonly calculated from MORB samples. Our

330   measurements and literature data are plotted in the εNd vs. εCe diagram (Fig. 2). The average of 48

331   MORB measurements gives εCe$_{DMM}$ = –1.1 ± 0.6 and εNd$_{DMM}$ = 9.7 ± 2.3. This mean Nd isotopic

332   composition is consistent with previously proposed values of 9.2 and 9.8 based on a more complete

333   dataset (Salters and Stracke, 2004, and Workman and Hart, 2005, respectively). Restricting the MORB

334   samples to those that do not show the Dupal anomaly (i.e., North Atlantic and Pacific MORBs) gives

335   an identical result (εCe = –1.2 ± 0.6, *n* = 33).

336

337   ***Continental Crust***

338   The CC is a low-mass reservoir containing 20–70% of the PM's incompatible element budget. The

339   difficulty in constraining the CC composition stems from its nature. With a mean age of 1.8–2.4 Ga

340   (Chauvel et al., 2014; Taylor and McLennan, 1995) and an average thickness of about 40 km, it is much

341   older and thicker than the present-day oceanic crust. The major- and trace-element compositions of the

342   upper, middle, and lower crust are based on numerous rock samples from which global compositions

343   were obtained (Rudnick and Gao, 2003, and references therein), though the isotopic composition of the

344   bulk CC is largely under-constrained; very few data are available for Ce, and εNd values generally vary

345   between –21 and –10. Based on loess measurements, Chauvel et al. (2014) proposed a model age of 1.8

346   Ga for the UCC and a εNd value of –10. On the other hand, Goldstein and Jacobsen (1988) considered

347   suspended materials in rivers (εNd = –11, T$_{DM}$ = 1.6 Ga) but corrected their mean value for the

348   preferential erosion of young terranes (εNd = –17 recalculated at 2.1 Ga). Similarly, Hawkesworth et al.

349   (2017) discussed the erosional bias based on the proportions of young and old source rocks and proposed

350   a bulk CC εNd value of –12. Other studies consider that the upper and bulk crusts have distinct isotope

351   signature; Allègre and Lewin (1989) calculated a εNd value of –21 from DMM-bulk CC mass-balance

352   equations, whereas Jacobsen and Wasserburg (1980) obtained a slightly higher value with a similar

353   approach (εNd = –14).

354

355   To date, CC rocks analysed for Ce and Nd isotopes are mainly ~2 Ga granites and gneisses (see

356   Supplementary Fig. S6 for details). Combining all published Ce-Nd measurements gives average values

357   of εCe = 2.8 and εNd = –19 (Fig. 4). This is slightly different from the sole published estimate for the

358   CC (εCe = 1.3 and εNd = –14; Tanaka et al., 1987), which was calculated by regression from five crustal

359   rock measurements (εCe = –0.112 × εNd) anchored to the mean εNd value of aeolian sediments and

360   particulates in rivers (εNd = –11.4; Goldstein et al., 1984). Our loess average is εCe = 1.8 and εNd = –

361   11.2, relatively close to Tanaka et al.'s (1987) value.

362

363   *Mafic crust*

364   Results obtained on the ^{146}Sm-^{142}Nd short-lived systematics suggest that the oldest mafic crust preserved

365   at the Earth's surface is the ~4.3 Ga Nuvvuagittuq Supracrustal Belt in northern Quebec (O'Neil et al.,

366   2008). Even if this age is debated, the neighbouring Hudson Bay terrane shows that the Archean felsic

367   crust formed by reworking of an Hadean mafic crust (O'Neil et al., 2019; O'Neil and Carlson, 2017).

368   We chose sample PC-162 (La/Ce = 0.49 and Sm/Nd = 0.27) as representative of the Archean mafic crust

369   to model its Ce and Nd isotopic compositions. This and other samples from the enriched low-Ti group

370   (O'Neil et al., 2011) are enriched in LREEs by 10 to 80 times the chondritic reference, whereas rocks

371   from the depleted low-Ti and high-Ti units show lower LREE enrichments (<20 times). Furthermore,

372   PC-162 is one of the most REE-depleted samples among those of the enriched low-Ti group that do not

373   show any evidence of metamorphic disturbance (O'Neil et al., 2012), and thus its REE contents

374   correspond to a reasonable crustal extraction rate: that is, more enriched compositions reflect increased

375   depletion of the mantle during extraction of the crust. The Ce-Nd isotopic compositions of the modelled

376   mafic end-member are reported in Figure 4; they are identical (εCe = 3.8 and εNd = –17.3) for a crust

377   formed at 4.3 Ga, irrespective of the PM considered (CHUR or EDR). The EER calculated by Carlson

378   and Boyet (2008) has similar La/Ce and Sm/Nd ratios of 0.47 and 0.28, respectively, producing present-

379   day isotopic compositions of εCe = 3 and εNd = –13.5 if this reservoir formed 4.3 Ga. Both these models

380   plot to the right of the mantle array (Fig. 4).

381

382   5.3.2. Model parameters and mixing hyperbolas

383

384   Our mass-balance models consider DMM-CC complementarity for chondritic and early-depleted PM

385   compositions. We aim to determine the εCe value of the CC using four-successive calculation steps

386   (Supplementary material). 1) We calculate the mass fraction of Nd in the CC relative to the total amount

387   in the crust and DMM (the sialic index; e.g., Allègre and Lewin, 1989) based on the DMM, CHUR/EDR

388   (Table 3), and CC εNd values. As the range of published CC isotopic values is large, we do not set a

389   precise εNd value in the mass-balance model, but consider all possibilities between εNd = –10 and –21.

390   2) We calculate the mass fraction of CC using the Nd contents of the BSE (as determined in section 5.2

391   with REE patterns anchored to a Lu content of 68 ppb; McDonough and Sun, 1995) and CC (Rudnick

392   and Gao, 2003). The Ce/Nd ratio is set to 1.28 for a chondritic BSE and to 1.22 for the EDR model

393   (Table 3). Importantly, the Lu value chosen to anchor the REE pattern of the BSE has no consequence

394   on the final εCe value. 3) The Ce sialic index is calculated using the Ce contents of the BSE (see step 2)

395   and CC (Rudnick and Gao, 2003). 4) The εCe value of the CC is calculated from the Ce sialic index and

396   the εCe values of the DMM and CHUR/EDR (Table 3): εCe_{CC} varies from 0.2 to 1 in the chondritic case

397   and from 0.4 to 1.2 in the EDR case. All CCs are represented as orange or green lines at the lower end

398   of the mixing curves in Figure 4 (chondritic or EDR model, respectively) and all calculated DMM-CC

399   mixing hyperbolas are plotted in the form of a coloured field. Their curvature is a function of the Ce/Nd

400   ratios of both end-members.

401

402   In the upper left of the εNd vs. εCe diagram, the DMM-CC mixing hyperbolas overlap and pass through

403   both the CHUR and EDR compositions. However, they do not fully overlap the data points defining the

404   mantle array. The Ce-Nd isotopic compositions calculated for the CC are always less radiogenic in

405   cerium than the mean values estimated from measurements, which might question the relevance of the

406   published data used to estimate the isotopic composition of the bulk CC. Most of the samples are upper

407   crust (e.g., loess) samples. If the observed difference reflects heterogeneities within the crustal reservoir,

408   the lower and middle crust should be characterised by negative εCe values to adjust the mass balance

409   budget within the continental crust (Willig and Stracke, 2019). However, Vervoort et al. (2000)

410   suggested that lower crustal xenoliths have εHf-εNd values close to the mantle array.

411

412   The mass fraction of depleted mantle relative to the whole mantle can be calculated in the case of the

413   mass balance calculations for the entire range of εNd_{CC} considered. It varies from 14 to 33% and from

414   28 to 64% ($\pm$20%) for the CHUR and EDR bulk compositions, respectively (Fig. 5). As mentioned in

415   section 5.3.1, a more depleted initial composition implies that a larger volume of the mantle was depleted

416   by crustal extraction (Boyet and Carlson, 2006). For comparison, Allègre and Lewin (1989) calculated

417   the mass fraction of depleted mantle to be comprised between 32 and 40% using a chondritic BSE.

418

419   The mixing curve joining the DMM and a 4.3 Ga early mafic crust is also reported in Figure 4. The

420   Ce/Nd ratio of this mafic crust is 1.9, only slightly different from the mean value of 2.15 determined for

421   the CC by Rudnick and Gao (2003). Thus, the DMM-mafic crust mixing hyperbola has a curvature close

422   to that of the DMM-CC mixing curve. Again, such a mixing scenario seems unlikely to reproduce the

423   mantle array.

424

425   5.3.3. What parameters can bring the DMM-CC mixing model closer to the mantle array?

426

427   To superimpose the DMM-CC mixing curve on the mantle array, Willig and Stracke (2019) proposed

428   using a more depleted isotopic composition for the DMM end-member (see their Figure 5). However,

429   for a likely CC Nd isotopic composition, such a DMM-CC hyperbola requires DMM Ce-Nd isotopic

430   ratios very different from those measured in MORB samples. For example, to fully reproduce the mantle

431   array, the εCe and εNd values of the DMM should be approximately –10 and +40, respectively, if we

432   set the εNd value of the bulk CC to –17 (in the case of a chondritic BSE). Such compositions have never

433   been measured in MORBs or peridotites.

434

435   Several authors have proposed loess samples to be a good approximation of the upper crust because

436   these clastic rocks sample large surface areas and have relatively uniform Nd and Hf isotopic

437   compositions (e.g., Chauvel et al., 2014). Because the lower crust appears to have Hf-Nd isotopic ratios

438   similar to those of the upper crust (Vervoort et al., 2000), we also calculated the εCe-εNd mixing

439   hyperbola between the DMM end-member and a loess-like component. Its curvature is a function of the

440   Ce/Nd ratios of both end-members. The mean Ce/Nd value calculated from our loess samples (2.38 ±

441   0.30) is similar within errors to the value of 2.33 determined for the upper crust by Rudnick and Gao

442   (2003) and to that of the global subducting sediment reservoir that represents the bulk composition of

443   trench sediments (Plank, 2014). However, this result is more than twice the Ce/Nd ratios of 1.08 and

444   0.95 determined for the DMM by Salters and Stracke (2004) and Workman and Hart (2005),

445   respectively. Consequently, considering the Ce-Nd isotopic composition of loess as representative of

446   the CC moves the DMM-CC mixing curve further from the mantle array (Fig. 4).

447

448   The model age of loesses is 1.8 Ga (Chauvel et al., 2014), which is not widely agreed to be the mean

449   age of the crust. An older equivalent (2.2 Ga) of these samples would have a less radiogenic Ce-Nd

450   isotopic composition that still plots on the mantle array. Superimposing the DMM-loess mixing curve

451   on the mantle array (i.e., to linearise the DMM-loess hyperbola) requires increasing the DMM Ce/Nd

452   ratio towards a value identical to that of loesses. Unlike the CC reservoir, which has been calculated

453   from a large number of measurements, the DMM remains a model based on a series of assumptions,

454   such that its REE pattern can be questioned. Such a reservoir is represented in MORB Ce and Nd isotopic

455   compositions as a strong long-term depleted REE element pattern, and a consistent Ce/Nd_{DMM} ratio

456   requires the DMM to have a positive Ce elemental anomaly. Cerium anomaly generally reflects a

457   specific behaviour of Ce^{4+} relative to REE^{3+}. However, such a Ce anomaly has never been measured in

458   MORBs.

459

460   The DMM-loess mixing curve coincides with the repartition of Island Arc Basalts (IABs) from the

461   Lesser Antilles and the Mariana Islands (Bellot et al., 2015, 2018). The isotopic compositions of OIBs

462   and IABs differ from those of MORBs due to the introduction of crustal material into their sources.

463   Although the isotopic compositions of arc lavas can be modified by post-melting reactions such as

464   assimilation-fractional crystallisation processes (AFC), this is not the case for the Marianas and Lesser

465   Antilles (e.g., Labanieh et al., 2010), and their Ce-Nd isotopic compositions are well explained by the

466   incorporation of sediments into the mantle wedge (Bellot et al., 2015, 2018). We expect a larger

467   incorporation of sediments in arc lavas relative to hotspot lavas since REEs are enriched in slab

468   dehydration fluids, whereas sediments are recycled with oceanic crust into the OIB source and their

469   signatures are consequently diluted. Indeed, OIBs and IABs are clearly distinct in the εCe-εNd diagram

470   (Fig. 4).

471

472

473   5.4. Effect of recycled surface material on the mantle array

474

475   The EM1, EM2, and HIMU mantle end-members have been defined from the most extreme isotopic

476   compositions measured in OIBs (Zindler and Hart, 1986) and are classically interpreted as representing

477   the recycling of surface materials into the deep mantle. Chauvel et al. (2008) modelled the Hf and Nd

478   isotopic compositions of basaltic crust and sediments recycled at different times during Earth's history

479   and showed that the Hf-Nd mantle array required the incorporation of surface material older than 2 Ga

480   into the OIB source. Here we apply the evolution model to the Ce-Nd systematics (see Supplementary

481   Fig. S7): 1) the isotopic composition of recycled sediments and recycled oceanic crust (ROC) calculated

482   back in time is assumed to be on the evolution line built between their present-day isotopic composition

483   and the CHUR value at 4.568 Ga; 2) the actual isotopic compositions of these two reservoirs are then

484   calculated considering the parent/daughter ratios in their source reservoirs. To this end, we consider the

485   mean $^{143}Nd/^{144}Nd$, $^{138}Ce/^{142}Ce$, $^{147}Sm/^{144}Nd$, and $^{138}La/^{142}Ce$ ratios measured in oceanic sediments in

486   front of the Mariana trench (Sites 801 and 802, ODP Leg 129; Bellot et al., 2018) and near the Lesser

487   Antilles arc (DSDP site 144; Bellot et al., 2015) together with those of the MORB samples plotted in

488   Figure 2. Modern oceanic sediments are characterised by negative elemental cerium anomalies,

489   reflecting an oxidised environment. Before the GOE, dated around 2.4 Ga (see Holland, 2002), all REEs

490   in sediments were necessarily trivalent under the anoxic conditions. Thus, we removed the elemental

491   cerium anomaly from all oceanic sediments older than 2.4 Ga.

492

493   Our calculations produce important results. First, the ROC follows a positive slope in the εCe-εNd

494   diagram, whereas the mantle array defines a negative slope (Fig. 6, see Supplementary Fig. S7 for further

495   details). Thus, the incorporation of ROC into the mantle tends to shift the isotopic composition of OIBs

496   toward slightly less radiogenic Ce isotopic ratios than MORBs. Second, as previously shown by Chauvel

497   et al. (2008), the mantle array can be reproduced by mixing either a DMM-like or a FOZO-like

498   component (FOZO is assumed to have εCe = –0.6 and εNd = 6.24; see Boyet et al., 2019) and recycled

499   surface material (ROC and sediments have the same recycling ages). On the sole basis of Ce and Nd

500   isotopes, it is still unclear whether the different plume sources contain surface material recycled at

501   various time or pre-GOE material in various proportions (the two propositions being not mutually

502   exclusive). Also, the intersections of the recycled crust-sediment mixing curves and the mantle array

503   indicate the proportion of sediments in the recycled material ($m_{sediments}$ / ($m_{sediments}$ + $m_{oceanic\ crust}$)) to be

504   between 6 and 12%; this proportion decreases for younger recycled components. This last result must

505   be considered in parallel with the decreasing rate of crustal destruction until the present value of 3.2–

506   5.5 km^3 yr^{-1} (Dhuime et al., 2018, and references therein).

507

508   Sediments formed before and after the GOE evolved to distinct Ce isotopic compositions. For a similar

509   proportion of sediments in the recycled component (i.e., 10% sediment and 90% oceanic crust), the εCe

510   value of a 2.5 Ga recycled component is inferior by 0.3 ε-units when we remove the Ce anomaly. More

511   importantly, in our model, only the recycling of pre-GOE sediments can explain the most enriched

512   isotopic compositions measured in OIBs. Corresponding samples are classified either as EM1 (samples

513   from Tristan Da Cunha, Gough, Heard, and Kerguelen Islands) or EM2 (Tahaa Island in the Society

514   archipelago). The Ce-Nd isotopic composition of Gough Island lavas was explained by the incorporation

515   of subcontinental lithospheric material at shallow depths into the mantle (Boyet et al., 2019). The lack

516   of correlation between the cerium anomalies and the Ce isotope compositions measured in Gough Island

517   lavas proves that ancient sediments carrier of negative element cerium anomaly were not incorporated

518   in the Gough mantle source. Moreover, mass-independent S isotopic fractionations measured in olivine-

519   hosted sulphides from other EM1 (e.g., Pitcairn) lavas similarly suggest the recycling of surface

520   materials that existed in a reduced atmosphere before the GOE (Cabral et al., 2013; Delavault et al.,

521   2016).

522

523

6. Conclusions

We measured the Ce isotopic compositions of 51 OIBs, 1 intraplate continental volcanism occurrence, 7 MORBs, 6 loess samples, and 11 chondrites, enhancing the terrestrial and extra-terrestrial Ce isotopic database. We define the $^{138}Ce/^{142}Ce$ CHUR reference to be 0.02256577 ± 66. OIB and MORB samples define the mantle array as $\varepsilon Nd = -7.3 (\pm 0.5) \times \varepsilon Ce + 0.4 (\pm 0.3)$. The mantle array passes through the CHUR value and is not significantly different from a modelled early-depleted reservoir. We conclude that combining Ce and Nd isotopic measurements in mantle-derived samples does not further constrain the composition of the PM.

Mixing models between the DMM and CC end members, both estimated from sample measurements (upper, or early mafic crusts), cannot reproduce the Ce-Nd mantle array but better fit IAB data. The mantle array is better reproduced by considering bulk CCs consistent with a mass-balance budget of the BSE (Ce isotopic compositions calculated for a range of accepted Nd). But the mixing hyperbolas do not perfectly overlap the OIB samples with subchondritic Ce isotopic composition; and the calculated εCe for the bulk crust are significantly different from all crustal rocks measured so far. In all these models, linearising the mixing curves requires unrealistic Ce-Nd isotopic compositions and/or Ce/Nd ratios never measured in rock samples. Alternatively, the recycling of sediments and oceanic crust into hotspot sources, and their mixing with DMM- or FOZO-like material may explain the Ce-Nd mantle array. Our results further show that Ce-Nd isotopic compositions measured in the most enriched EM-like lavas can be reproduced by the incorporation in their source of recycled oceanic sediments that do not have any elemental Ce anomaly. Because Ce is a redox-sensitive trace element that can be used to trace the oxygenation of atmosphere (GOE at 2.4 Ga), our results suggest that some OIBs sample very deep mantle reservoirs that may preserve pre-GOE recycled surface materials, in agreement with observed S isotopic fractions in EM1 lavas. Constraining the long-term history of recycled surface material in the mantle is essential to understand the isotope signature of mantle-derived samples. The La-Ce isotope systematics offers a unique opportunity to detect changes on the chemical composition of oceanic sediments through time.

569

570

Appendix A. Supplementary material

571

572

573   Supplementary material related to this article can be found online at XX.

574   Supplementary data 1: Major and trace element contents measured by quadrupole ICP-MS.

575   Supplementary data 2: Ce and Nd isotopic ratios of standard and rock samples and supplementary

576   information.

577 Supplementary material: 1) Sample descriptions from trace element diagrams and Ce anomalies; 2)

578 ^{138}Ce/^{142}Ce ratios from literature and example of normalisation with MORB; 3) ^{138}Ce/^{142}Ce ratios of

579 crustal samples from literature; 4) mass-balance calculations; and 5) recycling models.

580

581

References

583

584 Allègre, C.J., Lewin, É., 1989. Chemical structure and history of the Earth: evidence from global non-

585   linear inversion of isotopic data in a three-box model. Earth Planet. Sci. Lett. 96, 61–88.

586   https://doi.org/10.1016/0012-821X(89)90124-6

587 Allègre, C.J., Manhès, G., Lewin, É., 2001. Chemical composition of the Earth and the volatility

588   control on planetary genetics. Earth Planet. Sci. Lett. 185, 49–69. https://doi.org/10.1016/S0012-

589   821X(00)00359-9

590 Barrat, J.A., Zanda, B., Jambon, A., Bollinger, C., 2014. The lithophile trace elements in enstatite

591   chondrites. Geochim. Cosmochim. Acta 128, 71–94. https://doi.org/10.1016/j.gca.2013.11.042

592 Barrat, J.-A., Zanda, B., Moynier, F., Bollinger, C., Liorzou, C., Bayon, G., 2012. Geochemistry of CI

593   chondrites: Major and trace elements, and Cu and Zn isotopes. Geochim. Cosmochim. Acta 83,

594   79–92. https://doi.org/10.1016/j.gca.2011.12.011

595 Begemann, F., Ludwig, K.R., Lugmair, G.W., Min, K., Nyquist, L.E., Patchett, P.J., Renne, P.R.,

596   Shih, C.-Y., Villa, I.M., Walker, R.J., 2001. Call for an improved set of decay constants for

597   geochronological use. Geochim. Cosmochim. Acta 65, 111–121. https://doi.org/10.1016/S0016-

598   7037(00)00512-3

599 Bellot, N., Boyet, M., Doucelance, R., Bonnand, P., Savov, I.P., Plank, T., Elliott, T., 2018. Origin of

600   negative cerium anomalies in subduction-related volcanic samples: Constraints from Ce and Nd

601   isotopes. Chem. Geol. 500, 46–63. https://doi.org/10.1016/j.chemgeo.2018.09.006

602 Bellot, N., Boyet, M., Doucelance, R., Pin, C., Chauvel, C., Auclair, D., 2015. Ce isotope systematics

603   of island arc lavas from the Lesser Antilles. Geochim. Cosmochim. Acta 168, 261–279.

604   https://doi.org/10.1016/j.gca.2015.07.002

605   Belousova, E.A., Kostitsyn, Y.A., Griffin, W.L., Begg, G.C., O'Reilly, S.Y., Pearson, N.J., 2010. The

606   growth of the continental crust: Constraints from zircon Hf-isotope data. Lithos 119, 457–466.

607   https://doi.org/10.1016/j.lithos.2010.07.024

608   Blichert-Toft, J., Frey, F.A., Albarède, F., 1999. Hf Isotope Evidence for Pelagic Sediments in the

609   Source of Hawaiian Basalts. Science 285, 879. https://doi.org/10.1126/science.285.5429.879

610   Bonnand, P., Israel, C., Boyet, M., Doucelance, R., Auclair, D., 2019. Radiogenic and stable Ce

611   isotope measurements by thermal ionisation mass spectrometry. J. Anal. At. Spectrom.

612   https://doi.org/10.1039/C8JA00362A

613   Bouhifd, M.A., Boyet, M., Cartier, C., Hammouda, T., Bolfan-Casanova, N., Devidal, J.L., Andrault,

614   D., 2015. Superchondritic Sm/Nd ratio of the Earth: Impact of Earth's core formation. Earth

615   Planet. Sci. Lett. 413, 158–166. https://doi.org/10.1016/j.epsl.2014.12.054

616   Bouvier, A., Boyet, M., 2016. Primitive Solar System materials and Earth share a common initial

617   142Nd abundance. Nature 537, 399–402. https://doi.org/10.1038/nature19351

618   Bouvier, A., Vervoort, J.D., Patchett, P.J., 2008. The Lu–Hf and Sm–Nd isotopic composition of

619   CHUR: Constraints from unequilibrated chondrites and implications for the bulk composition of

620   terrestrial planets. Earth Planet. Sci. Lett. 273, 48–57. https://doi.org/10.1016/j.epsl.2008.06.010

621   Boyet, M., Bouvier, A., Frossard, P., Hammouda, T., Garçon, M., Gannoun, A., 2018. Enstatite

622   chondrites EL3 as building blocks for the Earth: The debate over the 146 Sm– 142 Nd

623   systematics. Earth Planet. Sci. Lett. 488, 68–78. https://doi.org/10.1016/j.epsl.2018.02.004

624   Boyet, M., Carlson, R.W., 2006. A new geochemical model for the Earth's mantle inferred from

625   146Sm–142Nd systematics. Earth Planet. Sci. Lett. 250, 254–268.

626   https://doi.org/10.1016/j.epsl.2006.07.046

627   Boyet, M., Carlson, R.W., 2005. 142Nd evidence for early (> 4.53 Ga) global differentiation of the

628   silicate Earth. Science 309, 576–581. https://doi.org/10.1126/science.1113634

629   Boyet, M., Doucelance, R., Israel, C., Bonnand, P., Auclair, D., Suchorski, K., Bosq, C., 2019. New

630   constraints on the origin of the EM-1 component revealed by the measurement of the La-Ce

631   isotope systematics in Gough Island lavas. Geochem. Geophys. Geosystems 20.

632   https://doi.org/10.1029/2019GC008228

633   Braukmüller, N., Wombacher, F., Hezel, D.C., Escoube, R., Münker, C., 2018. The chemical

634   composition of carbonaceous chondrites: Implications for volatile element depletion,

635   complementarity and alteration. Geochim. Cosmochim. Acta 239, 17–48.

636   https://doi.org/10.1016/j.gca.2018.07.023

637   Burkhardt, C., Borg, L.E., Brennecka, G.A., Shollenberger, Q.R., Dauphas, N., Kleine, T., 2016. A

638   nucleosynthetic origin for the Earth's anomalous 142Nd composition. Nature 537, 394–398.

639   https://doi.org/10.1038/nature18956

640   Cabral, R.A., Jackson, M.G., Rose-Koga, E.F., Koga, K.T., Whitehouse, M.J., Antonelli, M.A.,

641   Farquhar, J., Day, J.M.D., Hauri, E.H., 2013. Anomalous sulphur isotopes in plume lavas reveal

642   deep mantle storage of Archaean crust. Nature 496, 490. https://doi.org/10.1038/nature12020

643   Carlson, R.W., Boyet, M., 2008. Composition of the Earth's interior: the importance of early events.

644   Philos. Trans. R. Soc. Math. Phys. Eng. Sci. 366, 4077–4103.

645   https://doi.org/10.1098/rsta.2008.0166

646   Carlson, R.W., Boyet, M., Horan, M., 2007. Chondrite Barium, Neodymium, and Samarium Isotopic

647   Heterogeneity and Early Earth Differentiation. Science 316, 1175–1178.

648   https://doi.org/10.1126/science.1140189

649   Caro, G., Bourdon, B., Halliday, A.N., Quitté, G., 2008. Super-chondritic Sm/Nd ratios in Mars, the

650   Earth and the Moon. Nature 452, 336–339. https://doi.org/10.1038/nature06760

651   Carpentier, M., Chauvel, C., Maury, R.C., Mattielli, N., 2009. The "zircon effect" as recorded by the

652   chemical and Hf isotopic compositions of Lesser Antilles forearc sediments. Earth Planet. Sci.

653   Lett. 287, 86–99. https://doi.org/10.1016/j.epsl.2009.07.043

654   Chase, C., Patchett, P., 1988. Stored mafic/ultramafic crust and early Archean mantle depletion. Earth

655   Planet. Sci. Lett. 91, 66–72. https://doi.org/10.1016/0012-821X(88)90151-3

656   Chauvel, C., Garçon, M., Bureau, S., Besnault, A., Jahn, B., Ding, Z., 2014. Constraints from loess on

657   the Hf–Nd isotopic composition of the upper continental crust. Earth Planet. Sci. Lett. 388, 48–

658   58. https://doi.org/10.1016/j.epsl.2013.11.045

659   Chauvel, C., Lewin, E., Carpentier, M., Arndt, N.T., Marini, J.-C., 2008. Role of recycled oceanic

660   basalt and sediment in generating the Hf–Nd mantle array. Nat. Geosci. 1, 64–67.

661   https://doi.org/10.1038/ngeo.2007.51

662   Dauphas, N., 2017. The isotopic nature of the Earth's accreting material through time. Nature 541,

663   521–524. https://doi.org/10.1038/nature20830

664   Dauphas, N., Pourmand, A., 2015. Thulium anomalies and rare earth element patterns in meteorites

665   and Earth: Nebular fractionation and the nugget effect. Geochim. Cosmochim. Acta 163, 234–

666   261. https://doi.org/10.1016/j.gca.2015.03.037

667   Delavault, H., Chauvel, C., Thomassot, E., Devey, C.W., Dazas, B., 2016. Sulfur and lead isotopic

668   evidence of relic Archean sediments in the Pitcairn mantle plume. Proc. Natl. Acad. Sci. 113,

669   12952. https://doi.org/10.1073/pnas.1523805113

670   Dhuime, B., Hawkesworth, C.J., Cawood, P.A., Storey, C.D., 2012. A Change in the Geodynamics of

671   Continental Growth 3 Billion Years Ago. Science 335, 1334.

672   https://doi.org/10.1126/science.1216066

673   Dhuime, B., Hawkesworth, C.J., Delavault, H., Cawood, P.A., 2018. Rates of generation and

674   destruction of the continental crust: implications for continental growth. Philos. Trans. R. Soc.

675   Math. Phys. Eng. Sci. 376, 20170403. https://doi.org/10.1098/rsta.2017.0403

676   Dickin, A.P., 1987. Cerium isotope geochemistry of ocean island basalts. Nature 326, 283–284.

677   https://doi.org/10.1038/326283a0

678   Goldstein, S.J., Jacobsen, S.B., 1988. Nd and Sr isotopic systematics of river water suspended

679   material: implications for crustal evolution. Earth Planet. Sci. Lett. 87, 249–265.

680   https://doi.org/10.1016/0012-821X(88)90013-1

681   Goldstein, S.L., O'Nions, R.K., Hamilton, P.J., 1984. A Sm-Nd isotopic study of atmospheric dusts

682   and particulates from major river systems. Earth Planet. Sci. Lett. 70, 221–236.

683   https://doi.org/10.1016/0012-821X(84)90007-4

684   Hawkesworth, C.J., Cawood, P.A., Dhuime, B., Kemp, T.I.S., 2017. Earth's Continental Lithosphere

685   Through Time. Annu. Rev. Earth Planet. Sci. 45, 169–198. https://doi.org/10.1146/annurev-earth-

686   063016-020525

687   Holland, H.D., 2002. Volcanic gases, black smokers, and the great oxidation event. Geochim.

688   Cosmochim. Acta 66, 3811–3826. https://doi.org/10.1016/S0016-7037(02)00950-X

689   Jackson, M.G., Jellinek, A.M., 2013. Major and trace element composition of the high 3He/4He

690   mantle: Implications for the composition of a nonchonditic Earth. Geochem. Geophys.

691   Geosystems 14, 2954–2976. https://doi.org/10.1002/ggge.20188

692   Jacobsen, S.B., Wasserburg, G.J., 1980. A two-reservoir recycling model for mantle-crust evolution.

693   Proc. Natl. Acad. Sci. 77, 6298. https://doi.org/10.1073/pnas.77.11.6298

694   Javoy, M., 1995. The integral enstatite chondrite model of the Earth. Geophys. Res. Lett. 22, 2219–

695   2222. https://doi.org/10.1029/95GL02015

696   Jones, R.E., van Keken, P.E., Hauri, E.H., Tucker, J.M., Vervoort, J., Ballentine, C.J., 2019. Origins of

697   the terrestrial Hf-Nd mantle array: Evidence from a combined geodynamical-geochemical

698   approach. Earth Planet. Sci. Lett. 518, 26–39. https://doi.org/10.1016/j.epsl.2019.04.015

699   Labanieh, S., Chauvel, C., Germa, A., Quidelleur, X., Lewin, E., 2010. Isotopic hyperbolas constrain

700   sources and processes under the Lesser Antilles arc. Earth Planet. Sci. Lett. 298, 35–46.

701   https://doi.org/10.1016/j.epsl.2010.07.018

702   Lyubetskaya, T., Korenaga, J., 2007. Chemical composition of Earth's primitive mantle and its

703   variance: 1. Method and results. J. Geophys. Res. Solid Earth 112.

704   https://doi.org/10.1029/2005JB004223

705   Makishima, A., Masuda, A., 1994. Ce isotope ratios of N-type MORB. Chem. Geol. 118, 1–8.

706   https://doi.org/10.1016/0009-2541(94)90166-X

707   McDonough, W.F., Sun, S.-S., 1995. The composition of the Earth. Chem. Geol. 120, 223–253.

708   https://doi.org/10.1016/0009-2541(94)00140-4

709   O'Neil, J., Carlson, R.W., 2017. Building Archean cratons from Hadean mafic crust. Science 355,

710   1199. https://doi.org/10.1126/science.aah3823

711   O'Neil, J., Carlson, R.W., Francis, D., Stevenson, R.K., 2008. Neodymium-142 Evidence for Hadean

712   Mafic Crust. Science 321, 1828–1831. https://doi.org/10.1126/science.1161925

713   O'Neil, J., Carlson, R.W., Papineau, D., Levine, E.Y., Francis, D., 2019. Chapter 16 - The

714   Nuvvuagittuq Greenstone Belt: A Glimpse of Earth's Earliest Crust, in: Van Kranendonk, M.J.,

715   Bennett, V.C., Hoffmann, J.E. (Eds.), Earth's Oldest Rocks (Second Edition). Elsevier, pp. 349–

716   374. https://doi.org/10.1016/B978-0-444-63901-1.00016-2

717   O'Neil, J., Carlson, R.W., Paquette, J.-L., Francis, D., 2012. Formation age and metamorphic history

718   of the Nuvvuagittuq Greenstone Belt. Precambrian Res. 220–221, 23–44.

719   https://doi.org/10.1016/j.precamres.2012.07.009

720   O'Neil, J., Francis, D., Carlson, R.W., 2011. Implications of the Nuvvuagittuq Greenstone Belt for the

721   Formation of Earth's Early Crust. J. Petrol. 52, 985–1009.

722   https://doi.org/10.1093/petrology/egr014

723   O'Neill, H.St.C., Palme, H., 2008. Collisional erosion and the non-chondritic composition of the

724   terrestrial planets. Philos. Trans. R. Soc. Math. Phys. Eng. Sci. 366, 4205–4238.

725   https://doi.org/10.1098/rsta.2008.0111

726   Palme, H., O'Neill, H., 2014. Cosmochemical Estimates of Mantle Composition. Elsevier.

727   https://doi.org/10.1016/B978-0-08-095975-7.00201-1

728   Plank, T., 2014. The chemical composition of subducting sediments. Treatise Geochem. 4, 607–629.

729   https://doi.org/10.1016/b978-0-08-095975-7.00319-3

730   Pourmand, A., Dauphas, N., Ireland, T.J., 2012. A novel extraction chromatography and MC-ICP-MS

731   technique for rapid analysis of REE, Sc and Y: Revising CI-chondrite and Post-Archean

732   Australian Shale (PAAS) abundances. Chem. Geol. 291, 38–54.

733   https://doi.org/10.1016/j.chemgeo.2011.08.011

734   Rudnick, R.L., Gao, S., 2003. Composition of the continental crust, in: Holland, H.D., Turekian, K.K.

735   (Eds.), Treatise on Geochemistry. Pergamon, Oxford, pp. 1–64.

736   Salters, V.J.M., Stracke, A., 2004. Composition of the depleted mantle. Geochem. Geophys.

737   Geosystems 5. https://doi.org/10.1029/2003GC000597

738   Shimizu, H., Tanaka, T., Masuda, A., 1984. Meteoritic 138Ce/142Ce ratio and its evolution. Nature

739   307, 251–252. https://doi.org/10.1038/307251a0

740   Tanaka, T., Shimizu, H., Kawata, Y., Masuda, A., 1987. Combined La–Ce and Sm–Nd isotope

741   systematics in petrogenetic studies. Nature 327, 113–117. https://doi.org/10.1038/327113a0

742   Tanimizu, M., 2000. Geophysical determination of the 138 La β− decay constant. Phys. Rev. C 62,

743   017601. https://doi.org/10.1103/PhysRevC.62.017601

744   Taylor, S.R., McLennan, S.M., 1995. The geochemical evolution of the continental crust. Rev.

745 Geophys. 33, 241. https://doi.org/10.1029/95RG00262

746 Tazoe, H., Obata, H., Gamo, T., 2007. Determination of cerium isotope ratios in geochemical samples

747 using oxidative extraction technique with chelating resin. J. Anal. At. Spectrom. 22, 616.

748 https://doi.org/10.1039/b617285g

749 Vervoort, J.D., Patchett, P.J., Albarède, F., Blichert-Toft, J., Rudnick, R., Downes, H., 2000. Hf–Nd

750 isotopic evolution of the lower crust. Earth Planet. Sci. Lett. 181, 115–129.

751 https://doi.org/10.1016/S0012-821X(00)00170-9

752 Willig, M., Stracke, A., 2019. Earth's chondritic light rare earth element composition: Evidence from

753 the Ce–Nd isotope systematics of chondrites and oceanic basalts. Earth Planet. Sci. Lett. 509, 55–

754 65. https://doi.org/10.1016/j.epsl.2018.12.004

755 Workman, R.K., Hart, S.R., 2005. Major and trace element composition of the depleted MORB mantle

756 (DMM). Earth Planet. Sci. Lett. 231, 53–72. https://doi.org/10.1016/j.epsl.2004.12.005

757 Zindler, A., Hart, S., 1986. Chemical geodynamics. Annu. Rev. Earth Planet. Sci. 14, 493–571.

758 https://doi.org/10.1146/annurev.ea.14.050186.002425

759

760

761 **Table captions**

762

763 Table 1. ^{138}Ce/^{142}Ce and ^{143}Nd/^{144}Nd isotopic ratios and La/Ce and Sm/Nd ratios of whole-rock OIBs,

764 MORBs and loesses. The Nd isotopic compositions of loess and Kerguelen samples (*) are from

765 Chauvel et al. (2014) and unpublished data from B. Moine, respectively. Epsilon values are normalised

766 according to the CHUR references defined for Ce in this study as $\varepsilon Ce = \left(\dfrac{\frac{^{138}Ce}{^{142}Ce}_{sample}}{\frac{^{138}Ce}{^{142}Ce}_{CHUR}} - 1 \right) \times 10,000$

767 and for Nd by Bouvier et al. (2008) as $\varepsilon Nd = \left(\dfrac{\frac{^{143}Nd}{^{144}Nd}_{sample}}{\frac{^{143}Nd}{^{144}Nd}_{CHUR}} - 1 \right) \times 10,000$. Errors correspond to

768 internal errors (2se).

769

770   Table 2. ^{138}Ce/^{142}Ce isotopic ratios and La/Ce whole-rock chondrites. Epsilon values are normalised

771   according to the CHUR references defined for Ce in this study as $\varepsilon\text{Ce} = \left(\dfrac{\frac{^{138}\text{Ce}}{^{142}\text{Ce}}_{sample}}{\frac{^{138}\text{Ce}}{^{142}\text{Ce}}_{CHUR}} - 1 \right) \times 10{,}000.$

772   Errors correspond to internal errors (2se).

773

774   Table 3. Elemental and isotopic compositions of Earth's main silicate reservoirs used in our calculations:

775   BSE, bulk silicate Earth; EDR, early depleted reservoir; DMM, depleted MORB mantle; CC, continental

776   crust; UCC, upper continental crust; and mafic crust. Errors are errors on data averages. No errors are

777   given for model-based isotopic compositions (EDR, aged UCC, and mafic crust). Values in italics refer

778   to literature data: CC Ce and Nd concentrations are from Rudnick and Gao (2003), concentrations for

779   the mafic crust are those measured in PC-162 from O'Neil et al., (2011), and BSE ^{143}Nd/^{144}Nd ratios

780   are from Bouvier et al. (2008). BSE range of Ce and Nd concentrations are modelled using Lu contents

781   from Allègre et al. (2001), Lyubetskaya and Korenaga (2007), McDonough and Sun (1995), Palme and

782   O'Neill (2014) and chondritic REE ratios (see supplementary material S4 for more details). Ce/Nd of

783   the BSE is constant and set to 1.28 (1.22 for EDR). DMM isotopic composition is the mean value of

784   data from this study, Bellot et al., 2015, 2018, Makishima and Masuda, 1994 and Willig and Stracke,

785   2019. UCC (1.8 Ga) Ce and Nd contents and isotopic compositions are the mean values of loess data

786   from this study. UCC (2.2 Ga) isotopic compositions are calculated by aging 1.8 Ga UCC.

787

788   **Figure captions**

789

790   Fig. 1. A) ^{138}Ce/^{142}Ce ratios measured in enstatite (green squares), ordinary (red diamonds), and

791   carbonaceous (black triangles) chondrites. Literature values are from Bellot et al. (2015, 'B et al. 15')

792   and Willig and Stracke (2019, 'W&S19'). Data from the literature are normalised to the Ce$_{LMV}$ reference

793   material from this study: ^{138}Ce/^{142}Ce$_{CeLMV}$/^{138}Ce/^{142}Ce$_{CeAMES}$ = 0.02257053/0.02257426 (Bonnand et al.,

794   2019). B) εCe ratios vs. La/Ce ratios of chondrites from Willig and Stracke (2019) and this study. Data

795   are normalised to the CHUR reference defined in these studies. The dashed line represents the 4.568 Ga

796   CHUR reference isochron.

797

798   Fig. 2. εNd vs. εCe of mantle-derived samples and loesses from this study (coloured symbols). Nd

799   isotopic compositions of loess and Kerguelen samples are from Chauvel et al. (2014) and B. Moine

800   (unpublished data), and Ce and Nd isotopic compositions of Gough samples are from Boyet et al. (2019).

801   Literature data are in grey (Bellot et al., 2015, 2018; Makishima and Masuda, 1994; Willig and Stracke,

802   2019). Error bars are 2se (internal error). Literature data are reported considering the epsilon values and

803   CHUR references measured in each study to limit any bias introduced by normalisation. The data from

804   Tanaka et al. (1987) are not included because we do not have the corresponding CHUR reference. The

805   mantle array is defined by regression on mantle-derived samples only. Its equation defined from 134

806   data is εNd = -7.3 (± 0.5) × εCe + 0.4 (± 0.3) (calculated with Isoplot$^®$ and considering errors of 0.25

807   and 0.10 for εCe and εNd, respectively).

808

809   Fig. 3. REE patterns normalised to a chondritic primitive mantle for a chondritic BSE model (orange)

810   and an EDR model with Sm/Nd = Sm/Nd$_{BSE}$ + 3.6% (green). The EDR REE pattern is calculated as

811   follows. 1) The REE patterns are anchored at Lu, the least incompatible REE. 2) The early depleted

812   εNd$_{present}$ value is calculated using the initial CHUR value (Bouvier et al., 2008) at 4.568 Ga and a Sm/Nd

813   ratio 3.6% above that of the BSE. 3) The early depleted ^{177}Hf/^{176}Hf ratio is deduced from the Hf-Nd

814   mantle correlation (εHf$_{present}$ = 1.59 × εNd$_{present}$ + 1.28; Chauvel et al., 2008). 4) The Lu/Hf ratio is

815   obtained by comparison of the initial ^{177}Hf/^{176}Hf$_{CHUR}$ ratio (Bouvier et al., 2008) and the early depleted

816   Hf isotopic composition calculated in step 3. That is, the Hf concentration is obtained from the known

817   Lu concentration set as the anchor point in step 1. 5) The Sm concentration is calculated from the Sm/Hf

818   ratio, which has a constant value of 1.44 in OIBs (Jackson and Jellinek, 2013). 6) The Nd concentration

819   is calculated from the Sm/Nd ratio (known after steps 2 and 5). 7) The La and Ce concentrations are

820   calculated using a binomial fit through the chondrite normalised Sm, Nd, and Lu concentrations (i.e.,

821   the equation of the La–Lu pattern is of the form $y = ax^2 + bx + c$, where x represents the REEs, numbered

822   1–15 for La–Lu).

823

Fig. 4. εNd vs. εCe measured in mantle-derived samples (see Fig. 2, with additional data for IABs from Bellot et al., 2015, 2018 and continental crust samples; see Supplementary Fig. S6). The global linear trend of the mantle array is shown as the black dashed line and intercepts the chondritic composition (εNd = 0.00, εCe = 0.07 ± 0.05 (2σ)). Large symbols represent terrestrial reservoirs. Note that mean loess corresponds to a 1.8 Ga UCC (T_{DM}); and we represent a 2.2 Ga UCC as a modelled composition (aged loess). The mean CC value is the mean value of continental samples averaged by location. The continental crust value published in Tanaka et al. (1987) is calculated from 5 measurements. The 4.3 Ga mafic crust composition results from an extraction model from the depleted mantle. The red field represents the DMM-UCC mixing curves. The brown field corresponds to the DMM-4.3 Ga mafic crust mixing curves. The fields correspond to the different curves calculated using DMM Ce and Nd concentrations given by Salters and Stracke, 2004 and Workman and Hart, 2005. The orange field represents all the DMM-CC mixing curves calculated for a chondritic BSE model (bulk crust compositions shown by the bold orange line). The green field represents all the DMM-CC mixing curves calculated for an EDR model (bulk crust compositions shown by the bold green line). See details in the text and calculation parameters in Table 3.

839

Fig. 5. Mass fraction of the depleted mantle relative to the primitive mantle (m_{DM}/m_{PM}, expressed in percent) vs. the εNd value of the bulk continental crust. Two cases are represented: DMM-CC mixing for a chondritic BSE (orange) and DMM-CC mixing for an EDR (green). Parameters used in the calculations are discussed in the text and reported in Table 3.

844

Fig. 6. εNd vs. εCe measured in mantle-derived samples compared with reservoir evolution models. The present-day average compositions of the recycled oceanic crust (ROC = MORB; this study) and oceanic sediments (Bellot et al., 2015, 2018) are shown as large symbols. Solid lines outline the present-day isotopic compositions of these reservoirs if formed at different ages. The yellow line shows the evolution of MORBs using mean La/Ce and Sm/Nd ratios of MORBs and the MORB source. Similarly, the blue and purple lines show the evolution of oceanic sediments with chondrite-normalised REE patterns

851   showing a Ce negative anomaly as observed in modern oceanic sediments (La/Ce = 0.57) or without a

852   Ce anomaly (La/Ce = 0.47), representing oceanic sediments formed in reduced conditions before the

853   GOE (~2.4 Ga), respectively. The Ce-Nd isotopic composition of the recycled material is shown by

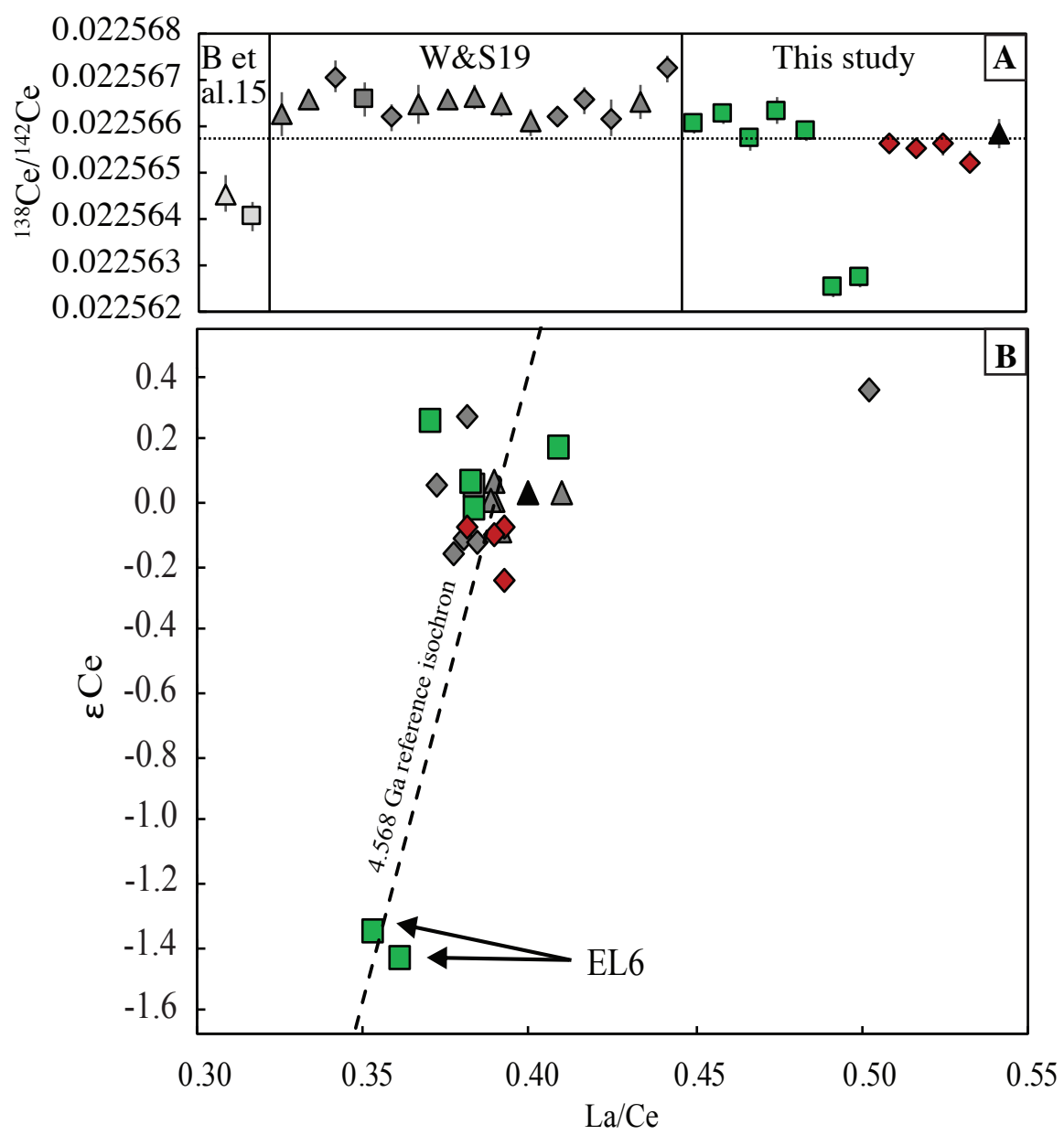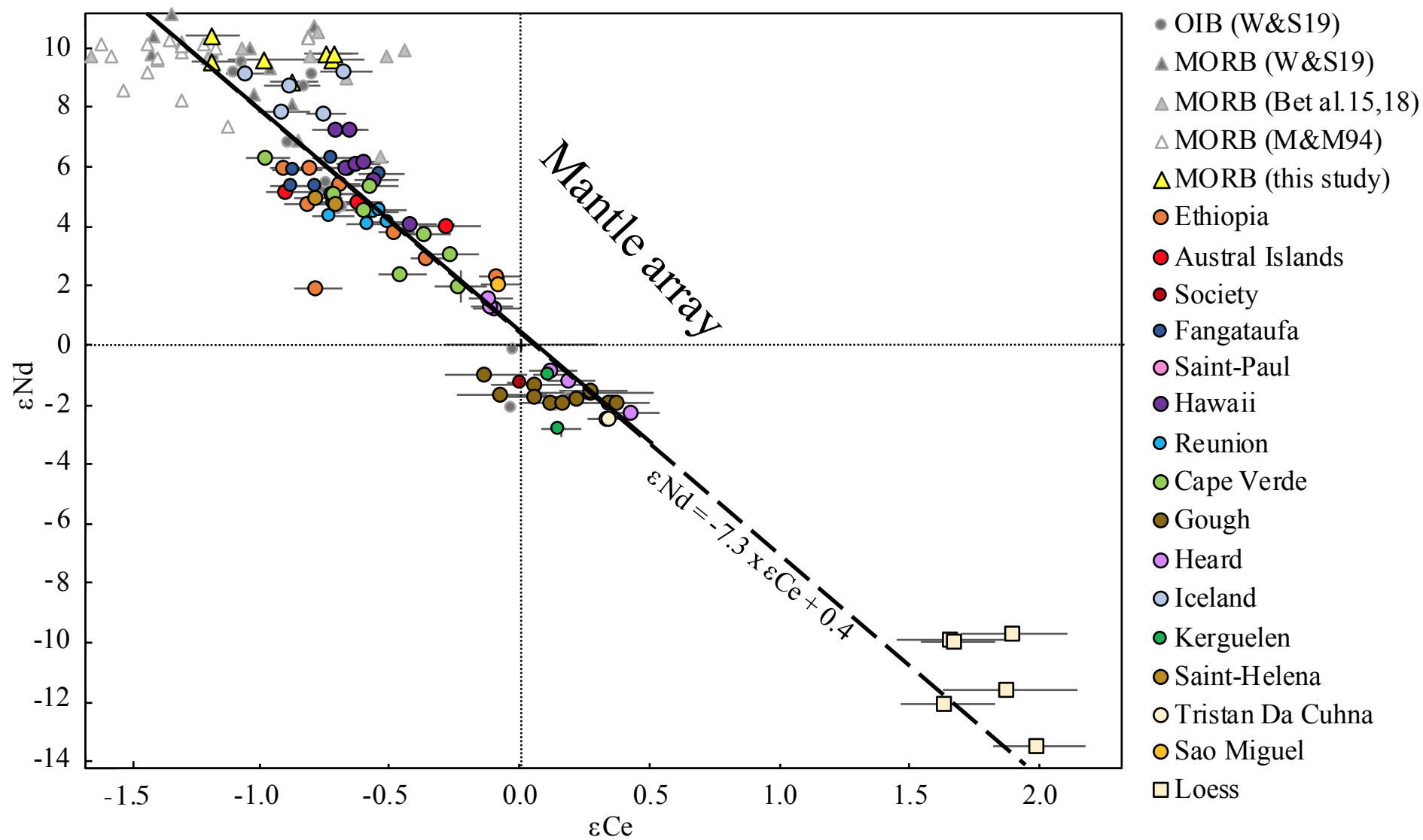854   mixing curves between contemporaneous ROC and oceanic sediments (dashed lines).
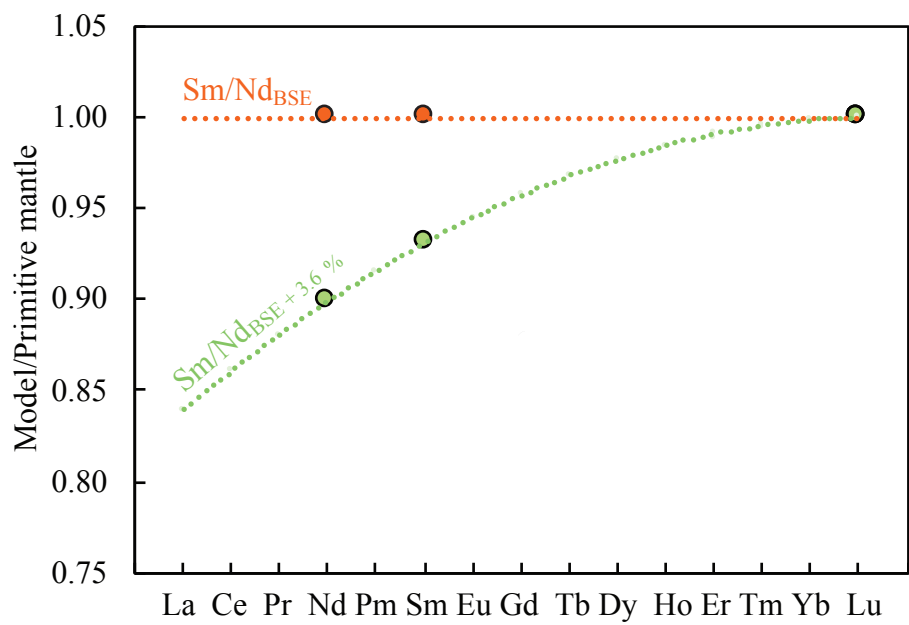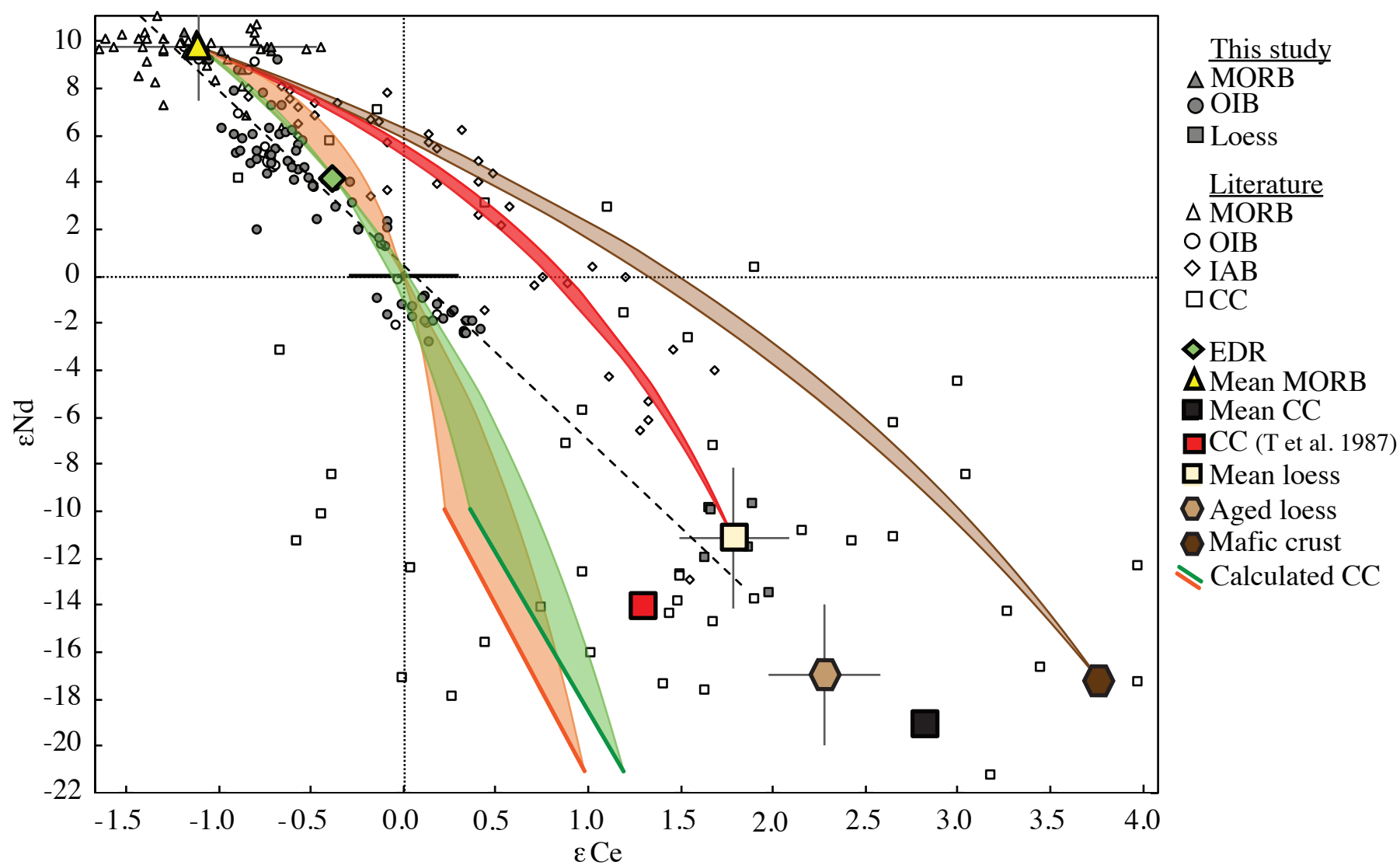
Fig.1

Fig.2

Fig.3

Fig.4
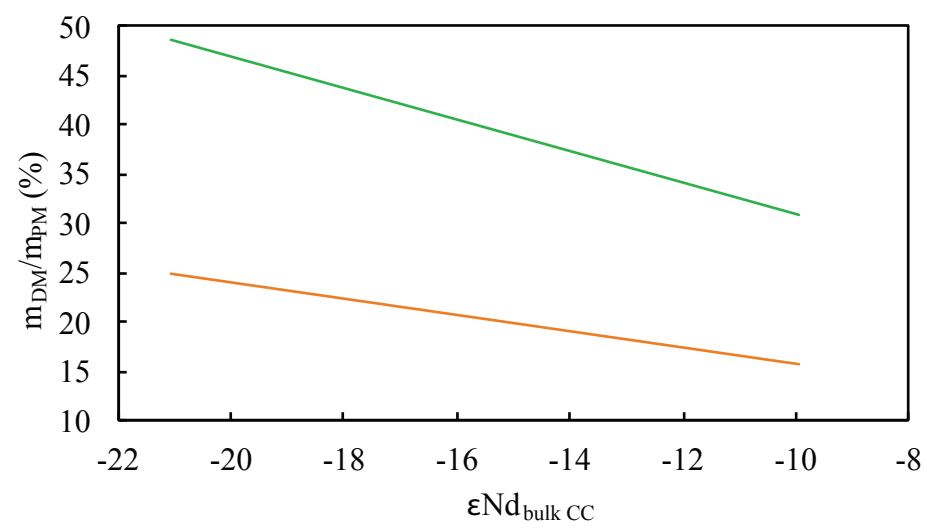
Fig.5
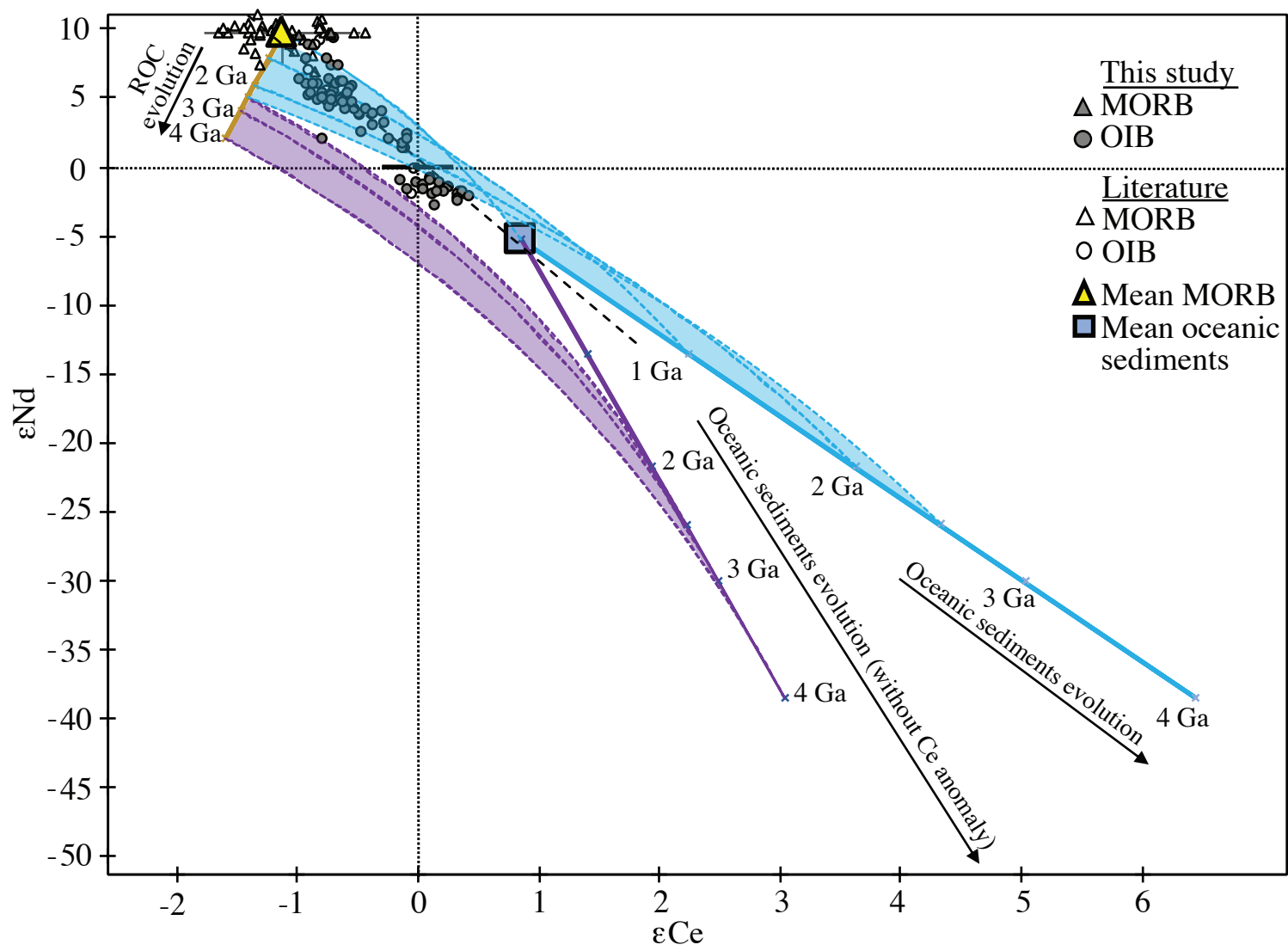
Fig.6

Table 1

Type	Sample	Location	Volcano	^{138}Ce/^{142}Ce	2se	εCe	La/Ce	^{143}Nd/^{144}Nd	2se	εNd	Sm/Nd
OIB	E38	Ethiopia		0.02256395	20	-0.81	0.305	0.512935	2	5.95	0.220
	E39			0.02256372	14	-0.91	0.318	0.512936	2	5.96	0.218
	E95			0.02256393	21	-0.81	0.318	0.512871	2	4.71	0.273
	E156			0.02256421	16	-0.69	0.375	0.512907	2	5.40	0.190
	E202			0.02256401	20	-0.78	0.310	0.512728	2	1.92	0.257
	E266			0.02256469	16	-0.48	0.399	0.512824	1	3.78	0.199
	E268			0.02256497	16	-0.35	0.459	0.512779	1	2.90	0.209
	E271			0.02256558	18	-0.08	0.478	0.512746	2	2.26	0.205
	RRTO 06	Austral Islands	Rututu	0.02256437	19	-0.62	0.474	0.512877	2	4.81	0.208
	TBA-IH		Tubuai	0.02256375	20	-0.89	0.355	0.512894	2	5.15	0.193
	MCD201		McDonald	0.02256514	27	-0.28	0.145	0.512834	2	3.98	0.280
	13K	Society	Tahaa	0.02256578	14	0.00	0.361	0.512563	2	-1.30	0.261
	F107	Tuamotu		0.02256382	22	-0.86	0.440	0.512929	2	5.83	0.236
	F124			0.02256379	21	-0.87	0.443	0.512902	2	5.30	0.219
	F128		Fangataufa	0.02256456	20	-0.53	0.460	0.512923	1	5.73	0.239
	F129			0.02256415	20	-0.72	0.436	0.512951	2	6.25	0.229
	F176			0.02256400	25	-0.78	0.494	0.512902	2	5.31	0.210
	SP1	St-Paul		0.02256416	16	-0.71	0.445	0.512876	2	4.79	0.251
	1804-1	Hawaii	Loihi	0.02256428	15	-0.66	0.295	0.512934	1	5.94	0.249
	1804-21			0.02256427	20	-0.66	0.308	0.512935	2	5.96	0.240
	1804-19			0.02256435	19	-0.63	0.275	0.512940	1	6.04	0.247
	Haw-2000-04		Mauna Loa	0.02256451	20	-0.55	0.387	0.512913	1	5.52	0.282
	Haw-2000-19			0.02256483	20	-0.41	0.401	0.512838	2	4.06	0.270
	Haw-2000-13		Kohala	0.02256417	22	-0.71	0.417	0.512999	1	7.20	0.214
	Haw-2000-28		Kilauea	0.02256442	20	-0.60	0.407	0.512944	2	6.13	0.285
	Haw-2000-17		Mauna Kea	0.02256430	15	-0.65	0.414	0.513000	1	7.21	0.233
	0608-021	Reunion	Piton de la	0.02256414	19	-0.72	0.436	0.512851	2	4.32	0.236
	80-76		Fournaise	0.02256463	18	-0.50	0.446	0.512841	2	4.11	0.229
	989/036			0.02256450	19	-0.56	0.445	0.512859	2	4.46	0.242
	986/115			0.02256445	20	-0.58	0.440	0.512837	2	4.03	0.230
	070406-1			0.02256457	20	-0.53	0.429	0.512862	2	4.53	0.250
	67a	Cape Verde	Fogo	0.02256517	23	-0.26	0.459	0.512786	1	3.03	0.175
	F10			0.02256524	23	-0.23	0.475	0.512730	3	1.94	0.179
	F16			0.02256473	20	-0.46	0.466	0.512752	2	2.37	0.185
	CY-165			0.02256448	23	-0.57	0.421	0.512901	1	5.30	0.186
	SV-01		Sao Vicente	0.02256415	20	-0.72	0.456	0.512890	1	5.08	0.191
	SV-12			0.02256417	22	-0.71	0.479	0.512889	2	5.05	0.202
	S-06		Sal	0.02256442	20	-0.60	0.469	0.512862	2	4.53	0.214
	SN-09		Sao Nicolau	0.02256356	19	-0.98	0.481	0.512952	2	6.29	0.190
	ST08		Santiago	0.02256495	21	-0.36	0.486	0.512822	1	3.74	0.200
	93(07)77	Iceland	Höfudreidarm	0.02256424	22	-0.67	0.336	0.513102	1	9.20	0.188
	93(07)76		úli	0.02256377	24	-0.88	0.359	0.513077	1	8.71	0.381
	93(07)24		Asbyrgi	0.02256408	17	-0.75	0.377	0.513027	2	7.74	0.352
	93(07)23			0.02256371	22	-0.91	0.372	0.513030	2	7.81	0.285
	93(07)56		Langaviti	0.02256340	20	-1.05	0.350	0.513097	1	9.12	0.298
	ACO 95-3	Sao Miguel		0.02256559	17	-0.08	0.479	0.512733	1	2.00	0.190
	BM1962 128 (114)	Tristan Da Cunha		0.02256653	19	0.34	0.448	0.512503	2	-2.47	0.178
	BM1962 128 (112)			0.02256654	18	0.34	0.489	0.512502	1	-2.49	0.178
	BM1965 P5 (8)	St-Helena		0.02256401	21	-0.78	0.741	0.512884	2	4.95	0.201
	BM1965 P5 (12)			0.02256417	18	-0.71	0.433	0.512872	2	4.73	0.208
	65001	Heard		0.02256604	20	0.12	0.456	0.512586	2	-0.87	0.203
	65151			0.02256674	22	0.43	0.468	0.512512	1	-2.31	0.198
	65171			0.02256620	21	0.19	0.545	0.512567	1	-1.23	0.188
	69230			0.02256555	22	-0.09	0.491	0.512691	3	1.19	0.184
	69244			0.02256551	18	-0.11	0.464	0.512697	2	1.30	0.196
	69254			0.02256550	20	-0.12	0.463	0.512711	2	1.57	0.195
	LVF-98-107	Kerguelen		0.02256577	23	0.00					
	MPC-99-103			0.02256611	17	0.15		0.512484*	12*	-2.85	
	RR08-121			0.02256603	17	0.12		0.512579*	2*	-0.99	
MORB	Searise-1 DR05-102	MORB	Pacific Ocean	0.02256309	23	-1.19	0.310	0.513164	2	10.42	0.349
	MD23 Site 4			0.02256380	21	-0.87	0.289	0.513084	1	8.85	0.308
	Clipperton DR01			0.02256355	33	-0.98	0.343	0.513122	2	9.59	0.321
	CY82-0903			0.02256310	20	-1.18	0.391	0.513118	1	9.52	0.278
	MD34-D3		Indian Ocean	0.02256414	27	-0.72	0.297	0.513122	2	9.60	0.393
	MD34-D4			0.02256409	22	-0.74	0.372	0.513133	1	9.81	0.336
	MD34-D6			0.02256416	20	-0.71	0.411	0.513133	1	9.81	0.305
Loess	R11	W Europe	Belgium	0.02257001	59	1.88		0.512035*	9*	-11.61	
	LO94		Svalbard	0.02257026	40	1.99		0.511937*	10*	-13.52	
	XN-4	China	Xining	0.02256952	50	1.66		0.512120*	11*	-9.95	
	Sahara 2900m	Sahara	Alpes, France	0.02256946	41	1.64		0.512011*	7*	-12.07	
	TJK3198	Tajikistan	Chashmanigar	0.02257004	46	1.89		0.512131*	8*	-9.73	
	TJK3165			0.02256955	32	1.68		0.512117*	9*	-10.01	

Table 2

Sample	Location	Type	$^{138}Ce/^{142}Ce$	2se	εCe	La/Ce
Sahara 97072	Sahara	EH3 - Find	0.02256613	21	0.16	0.410
Sahara 97158	Sahara	EH3 - Find	0.02256571	24	-0.02	0.385
Oudiyat Sbaa	W Sahara	EH5 - Fall	0.02256633	26	0.25	0.371
Adrar Bous	Niger	EL5 - Find	0.02256591	21	0.06	0.384
Yilmia	Australia	EL6 - Find	0.02256251	20	-1.44	0.362
Pillistfer	Estonia	EL6 - Fall	0.02256272	20	-1.35	0.354
Agen	France	H5 - Find	0.02256561	21	-0.07	0.393
NWA 8007	Morocco	L3 - Find	0.02256554	20	-0.10	0.389
NWA 10854	NW Africa	L3 - Find	0.02256560	23	-0.07	0.382
Saint-Severin	France	LL6 - Fall	0.02256522	23	-0.24	0.392
Allende	Mexico	CV3 – Fall	0.02256585	32	0.20	0.400

Table 3

	Chondritic BSE	EDR	DMM	CC	UCC (1.8 Ga)	UCC (2.2 Ga)	Mafic crust (4.3 Ga)
Ce (µg/g)	1.0-1.7			*43*	68	68	*11.2*
Nd (µg/g)	0.8-1.3			*20*	29	29	*5.9*
Ce/Nd	1.28	1.22		*2.15*	2.33	2.33	*1.9*
$^{138}Ce/^{142}Ce$	0.02256577 ± 66	0.02256492	0.02256325 ± 145		0.02256981 ± 68	0.02257091	0.0225743
εCe	0.00 ± 0.29	-0.4	-1.1 ± 0.6		1.8 ± 0.3	2.3	3.8
$^{143}Nd/^{144}Nd$	*0.512630 ± 11*	0.512842	0.513129 ± 116		0.512059 ± 155	0.511759	0.511745
εNd	*0.00 ± 0.21*	4.1	9.7 ± 2.3		-11.2 ± 3.0	-17	-17.3

Supplementary material

Formation of the Ce-Nd mantle array: crustal extraction vs. recycling by subduction

C. Israel[a,*], M. Boyet[a], R. Doucelance[a], P. Bonnand[a], P. Frossard[a], D. Auclair[a], A. Bouvier[b,c]

[a] Université Clermont Auvergne, CNRS, IRD, OPGC, Laboratoire Magmas et Volcans, F-63000 Clermont-Ferrand, France
[b] Department of Earth Sciences, Centre for Planetary Science and Exploration, University of Western Ontario, Ontario, Canada
[c] Bayerisches Geoinstitut, Universität Bayreuth, Germany

*Corresponding author.
E-mail address: claudine.israel@uca.fr (C. Israel).

Supplementary 1.
Trace element patterns and Ce anomalies
1. Trace element patterns
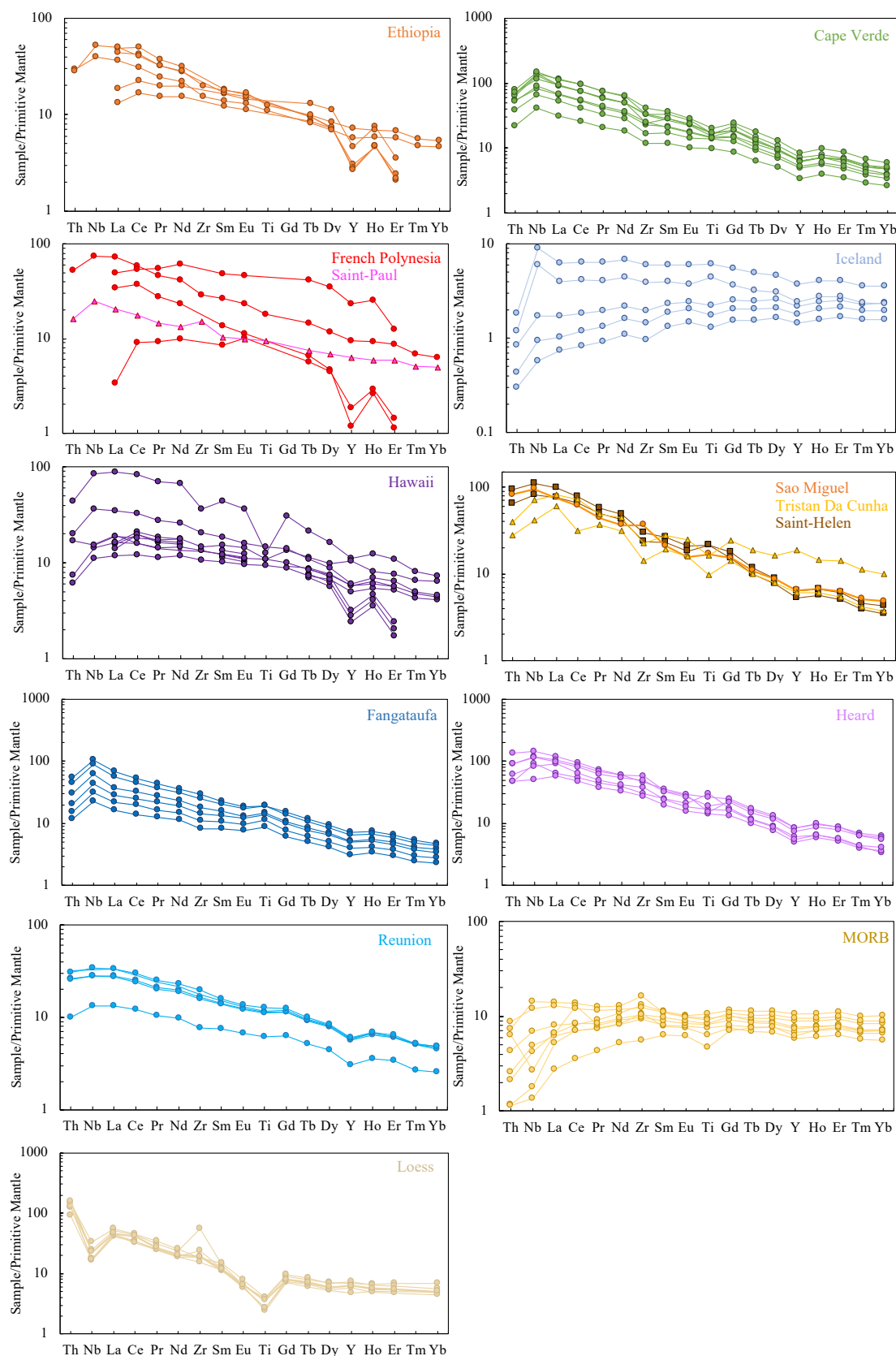
Fig. S1. Trace element patterns of OIBs, MORBs, and loesses. Concentrations are normalised to primitive mantle values (Sun and McDonough, 1989).
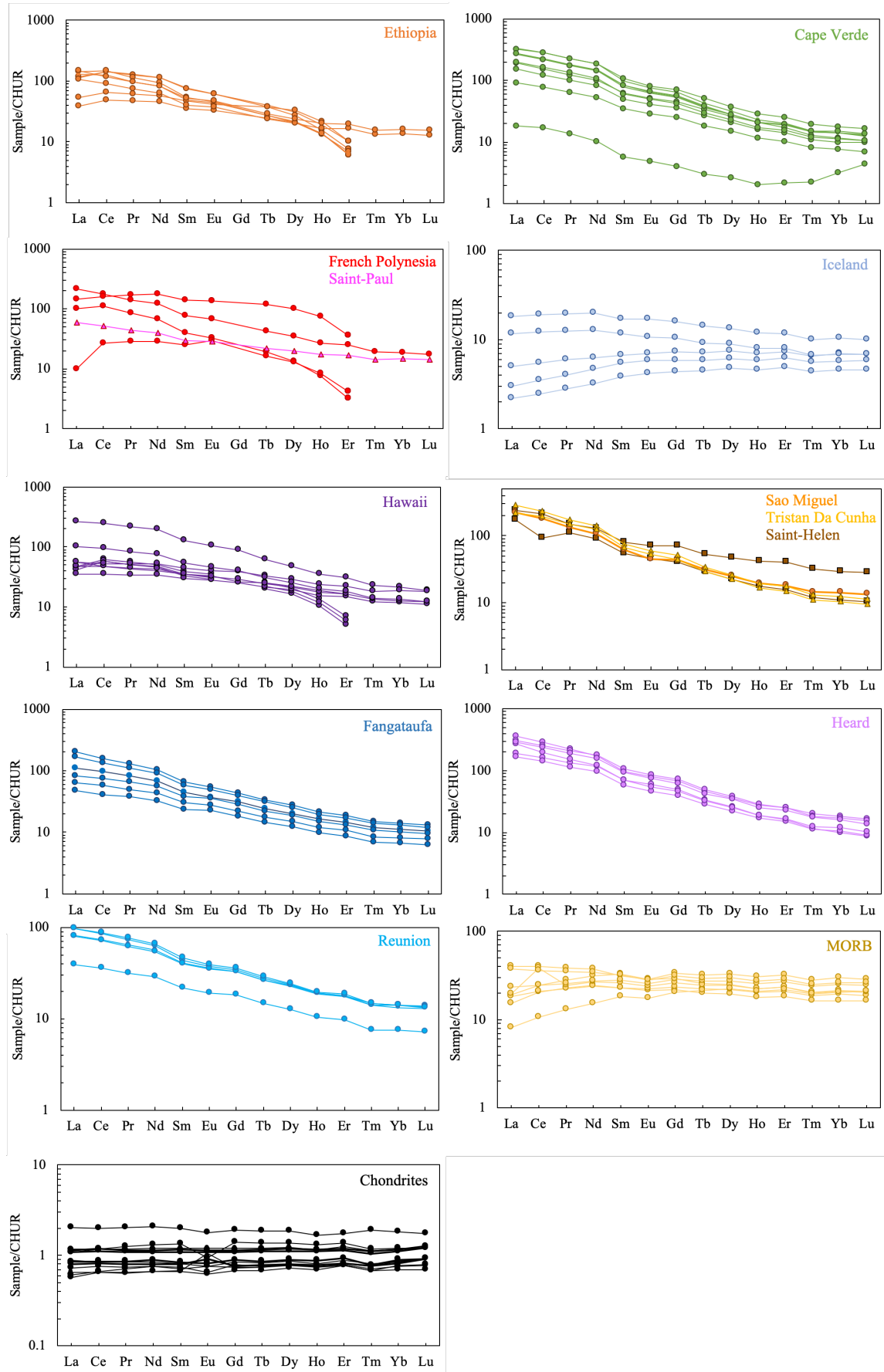
Fig S2. Rare earth element patterns of OIBs, MORBs, and chondrites. Concentrations are normalised to CI chondrite values (Barrat et al., 2012).

3
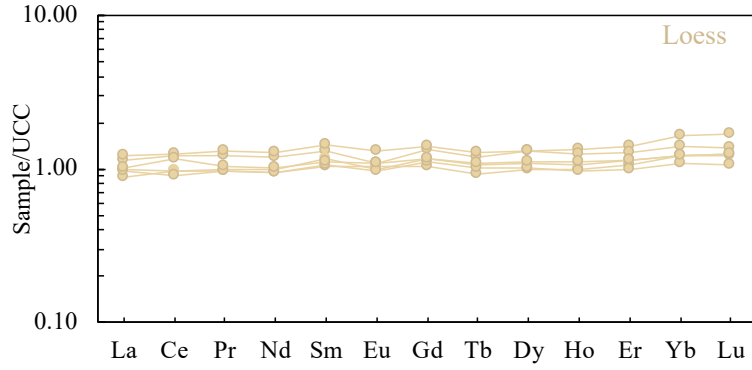
Fig. S3. Rare earth element patterns of loess samples. Concentrations are normalised to the upper continental crust (Rudnick and Gao, 2003).

2. Ce isotopic ratios as a function of elemental Ce anomalies
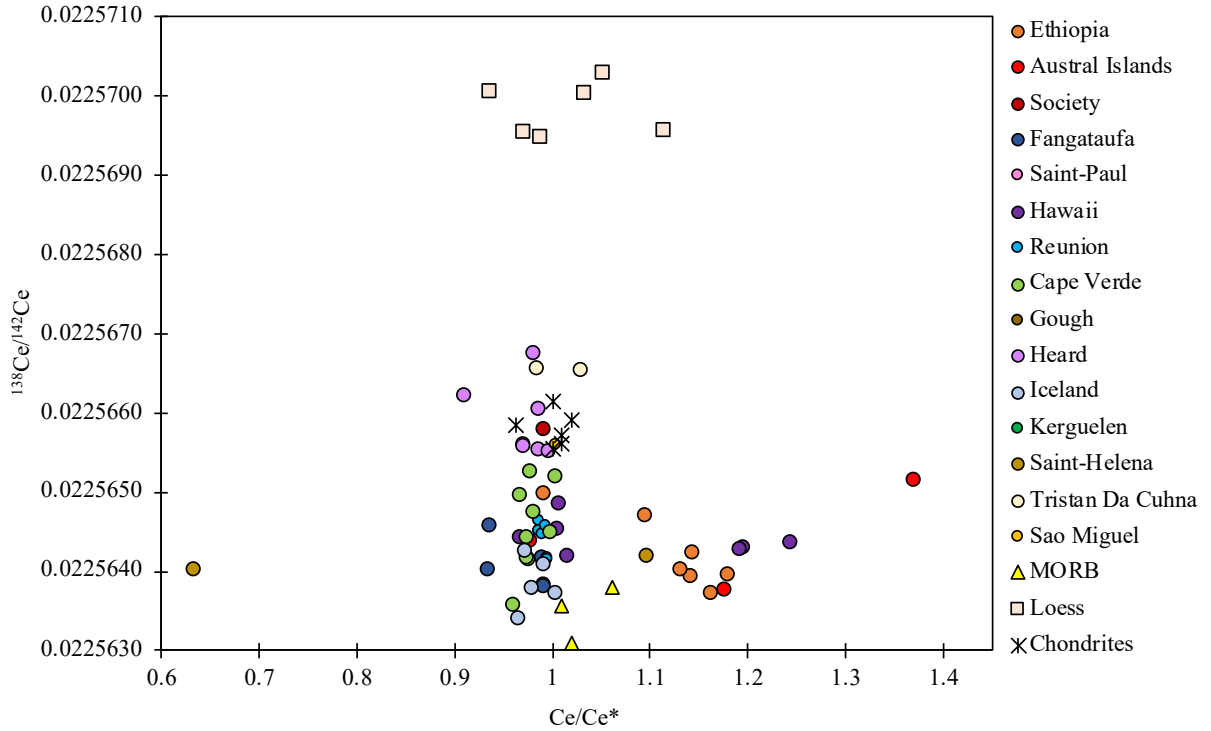
Fig. S4. $^{138}Ce/^{142}Ce$ vs Ce/Ce* diagram for terrestrial samples analysed in this study. Ce/Ce* represents the elemental Ce anomaly relative to the neighbouring REEs as $\frac{Ce}{Ce^*} = \frac{Ce_N}{\frac{1}{2}La_N + \frac{1}{2}Pr_N}$, where a_N, Ce_N, and Pr_N are the La, Ce, and Pr concentrations normalised to CI chondrite (Barrat et al., 2012). One sample from the Saint-Helena hotspot has a large negative Ce anomaly (Ce/Ce* = 0.64), but its Ce isotopic composition is similar to that of other samples from the same location. This anomaly probably reflects the late alteration of the rock. Some samples from Ethiopia, Hawaii, and French Polynesia have significant positive anomalies. These anomalies reflect depletion in La (Fig. S2), and are not correlated with Ce isotopic ratios.

We prefer to use the epsilon notation when comparing data from the literature. The most rigorous method for comparison is the use of CHUR values measured under the same analytical conditions (i.e., mass spectrometer, cup configuration, analytical protocol, etc.). This choice results from the difficulty in normalising data acquired with distinct protocols. In Fig. S5, we highlight the bias observed when comparing MORB samples from different studies (Bellot et al., 2015, 2018; Willig and Stracke, 2019) normalised using either BCR-2 or Ce$_{AMES}$. Isotopic compositions vary by up to 10 ppm for data from Willig and Stracke (2019) and by up to 20 ppm for data from Bellot et al. (2015, 2018).
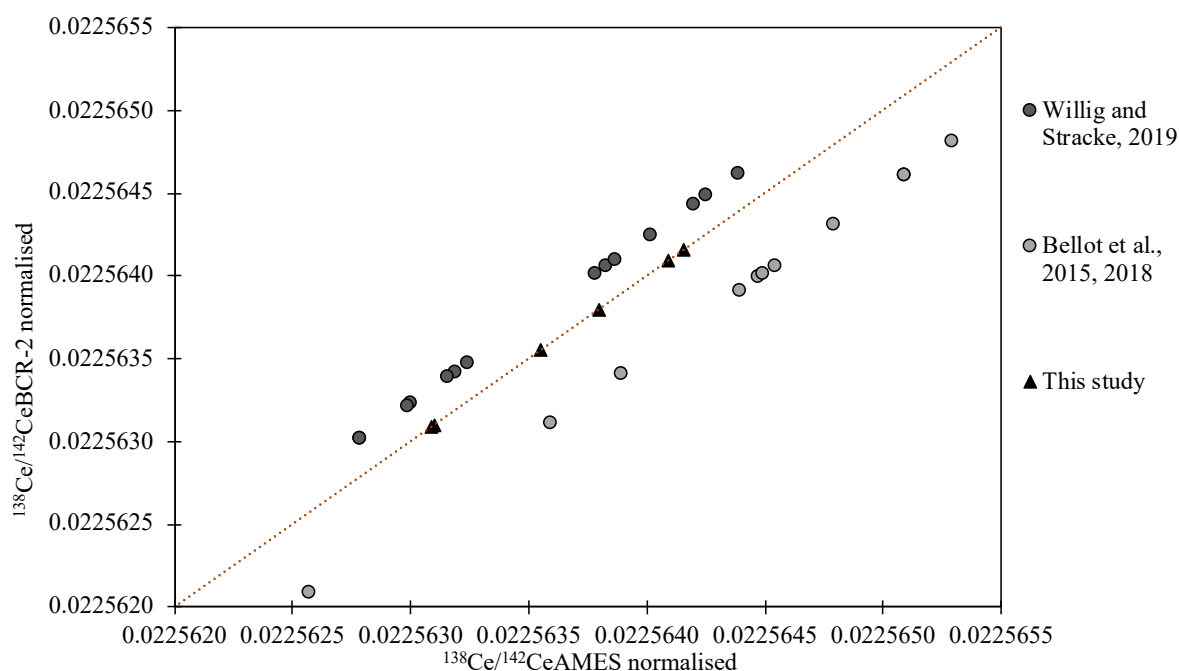
Fig. S5. Ce isotopic compositions of MORB samples from the literature normalised either to BCR-2 or to Ce$_{AMES}$ and compared to data from this study. The dotted line indicates the 1-1 correspondence line.

Supplementary 3.
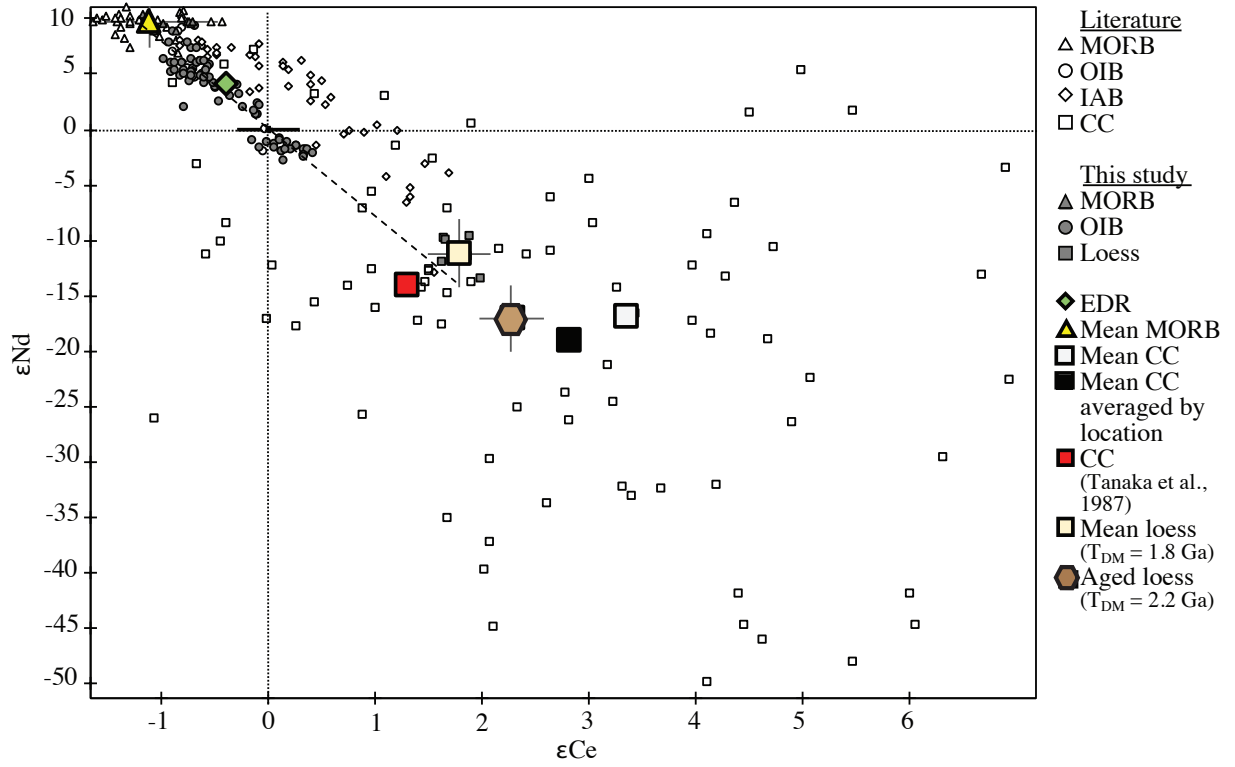## $^{138}Ce/^{142}Ce$ ratios of crustal samples from literature

Fig. S6. $^{143}Nd/^{144}Nd$ vs $^{138}Ce/^{142}Ce$ ratios measured in mantle-derived samples (see Fig. 2) and continental crust samples (Dickin et al., 1987; Gao et al., 2016; Hayashi et al., 2004; Lee et al., 2001, 2010; Liu et al., 1990; Masuda et al., 1988; Minami et al., 1995; Shimizu et al., 1988, 1990, 1996; Tanaka et al., 1987; Tazoe et al., 2007). Large symbols represent reservoirs (as in Fig. 6). Note that the red square is the continental crust proposed by Tanaka et al. (1987). The black square is the mean value of all literature continental crust samples represented here ($n = 94$), and the open square is the mean continental crust value when samples are averaged by location ($n = 16$).

Supplementary 4.
Mass-balance DMM-CC mixing calculations

Our single-stage differentiation model considers the continental crust (CC) and the depleted MORB mantle (DMM) to be complementary reservoirs developed from the primitive mantle (BSE).

The Nd sialic index (W_{Nd}) is defined as the amount of Nd in the continental crust relative to the total amount of Nd in the BSE (Allègre and Lewin, 1989). Its value can be obtained from the ^{143}Nd/^{144}Nd ratios of the BSE, DMM, and CC as:

$$\frac{143Nd}{144Nd}_{BSE} = W_{Nd} \times \frac{143Nd}{144Nd}_{CC} + (1 - W_{Nd}) \times \frac{143Nd}{144Nd}_{DMM}. \qquad (1)$$

The Nd sialic index can also be approximated as the product of the mass fraction of continental crust (W, relative to the BSE) and the ratio of the Nd contents in the continental crust and BSE as:

$$W_{Nd} = W \times \frac{[Nd]_{CC}}{[Nd]_{BSE}} \qquad \text{where } W = \frac{m_{cc}}{m_{CC}+m_{DMM}} \qquad . \qquad (2)$$

Using W as obtained above, the Ce sialic index (W_{Ce}) and the Ce isotopic composition of the continental crust can be deduced from equations similar to equations (1) and (2):

$$W_{Ce} = W \times \frac{[Ce]_{CC}}{[Ce]_{BSE}}, \qquad (4)$$

$$\frac{138Ce}{142Ce}_{BSE} = W_{Ce} \times \frac{138Ce}{142Ce}_{CC} + (1 - W_{Ce}) \times \frac{138Ce}{142Ce}_{DMM}. \qquad (3)$$

The mass fraction of continental crust W also allows us to recalculate the complementary Nd and Ce contents of the DMM using mass-balance equations for the trace element concentrations:

$$[Nd]_{BSE} = W \times [Nd]_{CC} + (1 - W) \times [Nd]_{DMM}, \qquad (5)$$

$$[Ce]_{BSE} = W \times [Ce]_{CC} + (1 - W) \times [Ce]_{DMM}. \qquad (6)$$

To maintain a consistent dataset between isotopic and elemental ratios, the Ce and Nd concentrations of the DMM are recalculated using the BSE and CC contents and the mass fraction of DMM determined in step 2 (= 1 – mass fraction of CC). The Ce/Nd ratio is set to 1.28 for a chondritic BSE and to 1.22 for the EDR model. So that the Lu value chosen to anchor the REE pattern of the BSE has no consequence on the final εCe value. Using the Lu contents proposed by Lyubetskaya and Korenaga (2007), Allègre et al. (2001), and Palme and O'Neill (2014) gives uncertainties of ±0.3 ppm on the Ce and Nd contents of the DMM. Corresponding DMM Ce and Nd concentrations are 0.1–1.0 and 0.6–1.0 ppm, respectively, in the chondritic case and 0.6–1.1 and 0.8–1.0 ppm, respectively, in the EDR model. We obtained restricted εNd$_{CC}$ ranges of –13 to –21 (CHUR) and –10 to –12 (EDR) that are similar within errors to the values proposed by Salters and Stracke (2004) and Workman and Hart (2005).
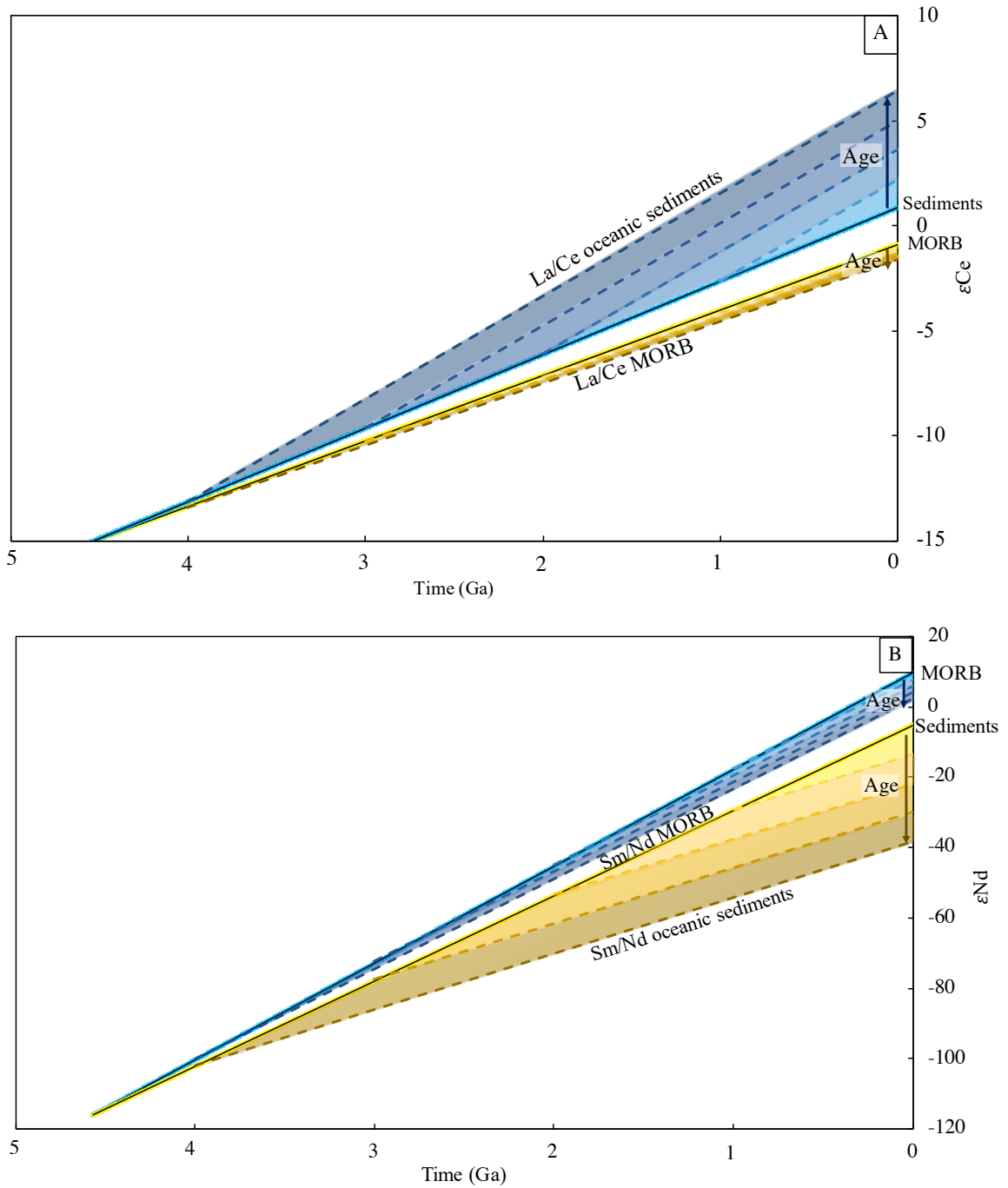
Supplementary 5.
Recycling models

Fig. S7. Evolution models used to calculate the present (A) εNd and (B) εCe isotopic compositions of recycled MORBs (yellow) and oceanic sediments (blue) for ages of formation between 4 and 1 Ga. Solid lines connect the present-day isotopic compositions of MORBs and oceanic sediments to the initial CHUR ratio, and dashed lines represent their isotopic evolution since the reservoir formation times. MORBs are characterised by $La/Ce_{MORB} = 0.34$ and $Sm/Nd_{MORB} = 0.33$ (this study). Oceanic sediments formed after the Great Oxygenation Event are characterised by $La/Ce_{OS} = 0.57$ and $Sm/Nd_{OS} = 0.20$ (data from Bellot et al., 2015, 2018), and those that formed earlier are assumed to have $La/Ce_{OS} = 0.47$ (after Ce anomaly correction). MORB and oceanic sediments sources have constant chemical ratios extrapolated from the evolution of an initial chondritic reservoir until present-day composition. MORB source has $La/Ce_{MORB\ source} = 0.36$ and $Sm/Nd_{MORB\ source} = 0.35$. Oceanic sediments source has $La/Ce_{sediments\ source} = 0.41$ and $Sm/Nd_{MORB\ source} = 0.31$. Figure modified after Chauvel et al. (2008).

	ROC (MORB)	MORB source	Oceanic sediments	Oceanic sediments (Pre-GOE)	Oceanic sediment source
La (µg/g)	5 ± 5		18 ± 9	18 ± 9	
Ce (µg/g)	15 ± 12		33 ± 25	38 ± 22	
La/Ce	0.34 ± 0.10	0.36	0.57 ± 0.25	0.47 ± 0.05	0.41
^{138}**Ce/**^{142}**Ce**	0.02256325 ± 145		0.02256771 ± 310	0.02256771 ± 310	
εCe	-1.1 ± 0.6		0.9 ± 1.4	0.9 ± 1.4	
Nd (µg/g)	13 ± 7		18 ± 13	18 ± 13	
Sm (µg/g)	4 ± 2		4 ± 3	4 ± 3	
Nd/Sm	0.34 ± 0.07	0.38	0.20 ± 0.03	0.20 ± 0.03	0.19
^{143}**Nd/**^{144}**Nd**	0.513129 ± 116		0.512360 ± 653	0.512360 ± 653	
εNd	9.7 ± 2.3		-5.3 ± 12.7	-5.3 ± 12.7	

Table S1: La, Ce, Sm and Nd contents, La/Ce and Sm/Nd ratios and Ce and Nd isotopic compositions of terrestrial reservoirs used in recycling models (Fig. 5 and Fig. S7). ROC, recycled oceanic crust; DMM, depleted MORB mantle; GOE, great oxygenation event. ROC and oceanic sediments isotopic and chemical compositions are based on measurements (MORB: this study, Bellot et al., 2015, 2018, Makishima and Masuda, 1994 and Willig and Stracke, 2019; oceanic sediments: Bellot et al., 2015, 2018). ROC and oceanic sediments sources have constant chemical ratios extrapolated from the evolution of an initial chondritic reservoir until present-day isotopic compositions measured in MORB and oceanic sediments. Pre-GOE oceanic sediments La/Ce ratio and Ce contents are corrected from Ce anomaly.

References :

Allègre, C.J., Lewin, É., 1989. Chemical structure and history of the Earth: evidence from global non-linear inversion of isotopic data in a three-box model. Earth Planet. Sci. Lett. 96, 61–88. https://doi.org/10.1016/0012-821X(89)90124-6

Barrat, J.-A., Zanda, B., Moynier, F., Bollinger, C., Liorzou, C., Bayon, G., 2012. Geochemistry of CI chondrites: Major and trace elements, and Cu and Zn isotopes. Geochim. Cosmochim. Acta 83, 79–92. https://doi.org/10.1016/j.gca.2011.12.011

Bellot, N., Boyet, M., Doucelance, R., Bonnand, P., Savov, I.P., Plank, T., Elliott, T., 2018. Origin of negative cerium anomalies in subduction-related volcanic samples: Constraints from Ce and Nd isotopes. Chem. Geol. 500, 46–63. https://doi.org/10.1016/j.chemgeo.2018.09.006

Bellot, N., Boyet, M., Doucelance, R., Pin, C., Chauvel, C., Auclair, D., 2015. Ce isotope systematics of island arc lavas from the Lesser Antilles. Geochim. Cosmochim. Acta 168, 261–279. https://doi.org/10.1016/j.gca.2015.07.002

Chauvel, C., Lewin, E., Carpentier, M., Arndt, N.T., Marini, J.-C., 2008. Role of recycled oceanic basalt and sediment in generating the Hf–Nd mantle array. Nat. Geosci. 1, 64–67. https://doi.org/10.1038/ngeo.2007.51

Dickin, A.P., Jones, N.W., Thirlwall, M.F., Thompson, R.N., 1987. A Ce/Nd isotope study of crustal contamination processes affecting Palaeocene magmas in Skye, Northwest Scotland. Contrib. Mineral. Petrol. 96, 455–464. https://doi.org/10.1007/BF01166690

Gao, Y., Ling, W., Qiu, X., Chen, Z., Lu, S., Bai, Xiao, Bai, Xiujuan, Zhang, J., Yang, H., Duan, R., 2016. Decoupled Ce-Nd isotopic systematics of the Neoproterozoic Huangling intrusive complex and its geological significance, eastern Three Gorges, South China. J. Earth Sci. 27, 864–873. https://doi.org/10.1007/s12583-016-0692-6

Hayashi, T., Tanimizu, M., Tanaka, T., 2004. Origin of negative Ce anomalies in Barberton sedimentary rocks, deduced from La–Ce and Sm–Nd isotope systematics. Precambrian Res. 135, 345–357. https://doi.org/10.1016/j.precamres.2004.09.004

Lee, S.-G., Asahara, Y., Tanaka, T., Kim, N.H., Kim, K.H., Yi, K., Masuda, A., Song, Y.S., 2010. La–Ce and Sm–Nd isotopic systematics of early Proterozoic leucogranite with tetrad REE pattern. Chem. Geol. 276, 360–373. https://doi.org/10.1016/j.chemgeo.2010.07.003

Lee, S.-G., Masuda, A., Shimizu, H., Song, Y.-S., 2001. Crustal evolution history of Korean Peninsula in East Asia: The significance of Nd, Ce isotopic and REE data from the Korean Precambrian gneisses. Geochem. J. 35, 175–187. https://doi.org/10.2343/geochemj.35.175

Liu, C.-Q., Shimizu, H., Nakai, S., Xie, G.-H., Masuda, A., 1990. Isotopic and trace element studies for Cenozoic volcanic rocks from western China: implication for a crust-like enriched component in the mantle. Geochem. J. 24, 327–342.

Masuda, A., Shimizu, H., Nakai, S., Makishima, A., Lahti, S., 1988. 138La β-decay constant estimated from geochronological studies. Earth Planet. Sci. Lett. 89, 316–322.

Minami, M., Shimizu, H., Masuda, A., Adachi, M., 1995. Two Archean Sm-Nd ages of 3.2 and 2.5 Ga for the Marble Bar Chert, Warrawoona Group, Pilbara Block, Western Australia. Geochem. J. 29, 347–362. https://doi.org/10.2343/geochemj.29.347

Rudnick, R.L., Gao, S., 2003. Composition of the continental crust, in: Holland, H.D., Turekian, K.K. (Eds.), Treatise on Geochemistry. Pergamon, Oxford, pp. 1–64.

Shimizu, H., Lee, S.-G., Masuda, A., Adachi, M., 1996. Geochemistry of Nd and Ce isotopes and REE abundances in Precambrian orthogneiss clasts from the Kamiaso conglomerate, central Japan. Geochem. J. 30, 57–69. https://doi.org/10.2343/geochemj.30.57

Shimizu, H., Nakai, S., Tasaki, S., Masuda, A., Bridgwater, D., Nutman, A., Baadsgaard, H., 1988. Geochemistry of Ce and Nd isotopes and REE abundances in the Amitsoq gneisses, West Greenland. Earth Planet. Sci. Lett. 91, 159–169.

Shimizu, H., Umemoto, N., Masuda, A., Appel, P.W.U., 1990. Sources of iron-formations in the archean isua and malene supracrustals, West Greenland: Evidence from La-Ce and sm-nd isotopic data and REE abundances. Geochim. Cosmochim. Acta 54, 1147–1154. https://doi.org/10.1016/0016-7037(90)90445-Q

Sun, S. -s., McDonough, W.F., 1989. Chemical and isotopic systematics of oceanic basalts: implications for mantle composition and processes. Geol. Soc. Lond. Spec. Publ. 42, 313–345. https://doi.org/10.1144/GSL.SP.1989.042.01.19

Tanaka, T., Shimizu, H., Kawata, Y., Masuda, A., 1987. Combined La–Ce and Sm–Nd isotope systematics in petrogenetic studies. Nature 327, 113–117. https://doi.org/10.1038/327113a0

Tazoe, H., Obata, H., Gamo, T., 2007. Determination of cerium isotope ratios in geochemical samples using oxidative extraction technique with chelating resin. J. Anal. At. Spectrom. 22, 616. https://doi.org/10.1039/b617285g

Willig, M., Stracke, A., 2019. Earth's chondritic light rare earth element composition: Evidence from the Ce–Nd isotope systematics of chondrites and oceanic basalts. Earth Planet. Sci. Lett. 509, 55–65. https://doi.org/10.1016/j.epsl.2018.12.004